Biomimetic Approaches for the Design and Fabrication of Bone-to-Soft Tissue Interfaces

Pitta Kruize, Carlos; Panahkhahi, Sara; Putra, Niko Eka; Diaz-Payno, Pedro; Van Osch, Gerjo; Zadpoor, Amir A.; Mirzaali, Mohammad J.

DOI
10.1021/acsbiomaterials.1c00620

Publication date
2023

Document Version
Final published version

Published in
ACS Biomaterials Science and Engineering

ACS Biomaterials SCIENCE & ENGINEERING

pubs.acs.org/journal/abseba

Review

Biomimetic Approaches for the Design and Fabrication of Bone-to-Soft Tissue Interfaces

Carlos Pitta Kruize, Sara Panahkhahi, Niko Eka Putra, Pedro Diaz-Payno, Gerjo van Osch, Amir A. Zadpoor, and Mohammad J. Mirzaali*

Cite This: *ACS Biomater. Sci. Eng.* 2023, 9, 3810−3831

Read Online

ACCESS | Metrics & More | Article Recommendations

ABSTRACT: Bone-to-soft tissue interfaces are responsible for transferring loads between tissues with significantly dissimilar material properties. The examples of connective soft tissues are ligaments, tendons, and cartilages. Such natural tissue interfaces have unique microstructural properties and characteristics which avoid the abrupt transitions between two tissues and prevent formation of stress concentration at their connections. Here, we review some of the important characteristics of these natural interfaces. The native bone-to-soft tissue interfaces consist of several hierarchical levels which are formed in a highly specialized anisotropic fashion and are composed of different types of heterogeneously distributed cells. The characteristics of a natural interface can rely on two main design principles, namely by changing the local microarchitectural features (*e.g.*, complex cell arrangements, and introducing interlocking mechanisms at the interfaces through various geometrical designs) and changing the local chemical compositions (*e.g.*, a smooth and gradual transition in the level of mineralization). Implementing such design principles appears to be a promising approach that can be used in the design, reconstruction, and regeneration of engineered biomimetic tissue interfaces. Furthermore, prominent fabrication techniques such as additive manufacturing (AM) including 3D printing and electrospinning can be used to ease these implementation processes. Biomimetic interfaces have several biological applications, for example, to create synthetic scaffolds for osteochondral tissue repair.

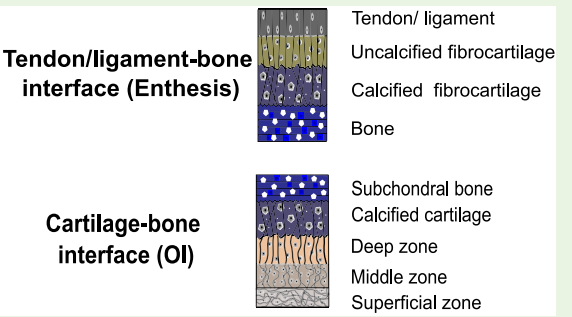

KEYWORDS: *biomimetics, bone−soft tissue interfaces, additive manufacturing, tissue interface engineering, functional gradient*

1. INTRODUCTION

Most of natural organisms consist of assemblages of hard and soft tissues. These hard−soft compartments can create interfaces that are functionally adaptive, sustainable, and less prone to failure. Therefore, they can be a source of inspiration for engineers and biologists who aim to design and build synthetic hard−soft interfaces (HSIs).

When joining two dissimilar materials, the elastic stiffness mismatches determine how effectively a contact between two materials can occur. This is due to the fact that the distinct deformation between the extreme hard−soft connection gives rise to interfacial stresses,[1] decreasing structural integrity and making the interface susceptible to failure.[2] In Nature, however, the union of two materials with nonidentical properties can be frequently seen. These natural interfaces provide structural and functional integration between different tissues,[3] where the mechanical properties can gradually change through variations in mineral contents and matrix compositions.[4] An example of such interfaces is the connection of bone that possesses an elastic stiffness of ∼20 GPa[5] to soft tissues such tendons and ligaments whose elastic stiffnesses are 2 to 3 orders of magnitude lower.[6]

Bone-to-soft tissue interfaces (BSTIs) are critical for the musculoskeletal system's complexity, which needs to ensure the efficiency of load transferring between distinct tissues. The microstructures of BSTIs are highly heterogeneous and anisotropic, consisting of gradual variations in materials composition from bone to soft tissues, as shown in Figure 1 for the human knee joint.[3,7] Although these interfaces are durable, they experience various defects over the life span of humans and can be damaged by loading, particularly when the joint interfaces are degenerated.[8] Failure of BSTIs usually leads to long-term injuries, as the healing process fails to regenerate the complexity of the native tissue interface.[9] Due to the inability of the body to regenerate the natural structure of the BSTIs, the scar tissues that form the interfaces and also the surgically repaired interfaces can both be susceptible to retear

Special Issue: Engineering Bioinspired and Biological Materials

Received: May 9, 2021
Accepted: November 4, 2021
Published: November 16, 2021

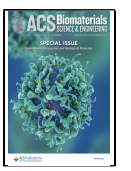

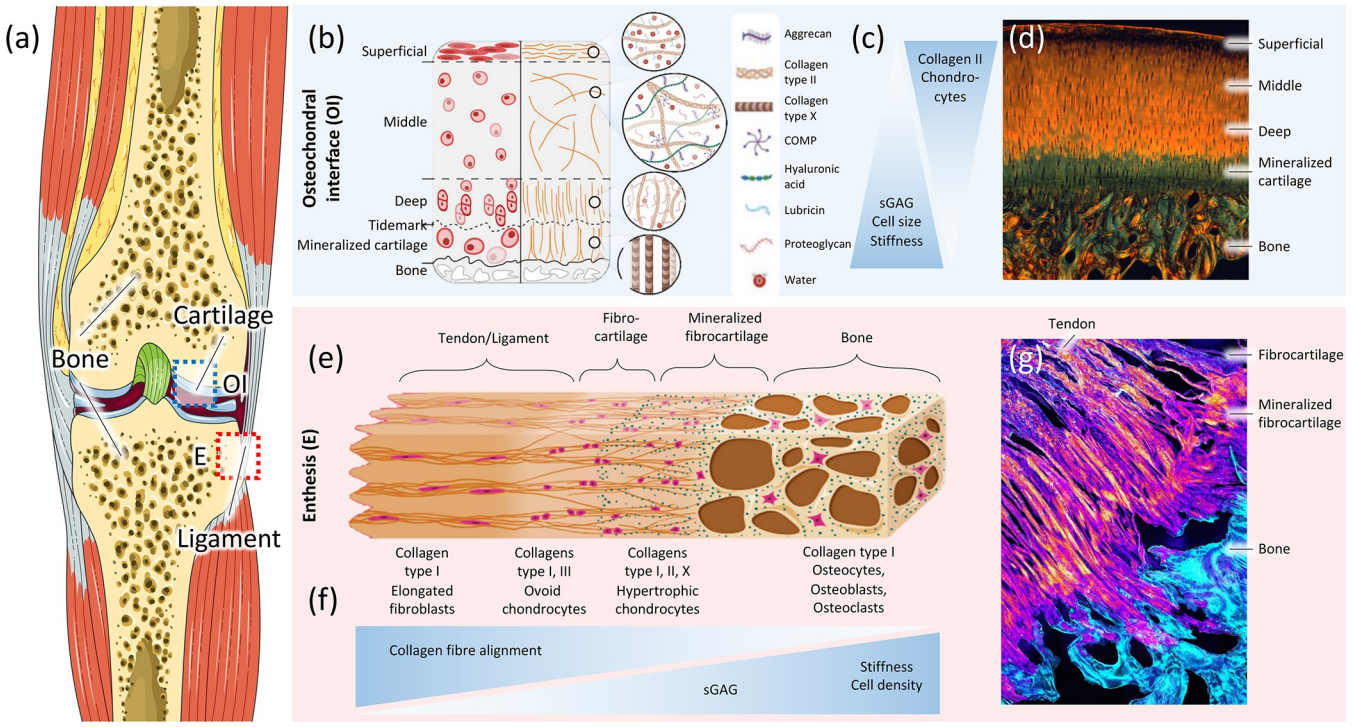

Figure 1. Structure of bone-to-soft interfaces in the human knee joint. (a) Human knee (from Servier Medical Art) illustrating a blue box for the osteochondral interface (OI) and a red box for the enthesis (E). (b) Schematic of the osteochondral interface divided into the morphology and distribution of the cells (left) and the matrix organization (right) within the different zones in the OI. Panel b is reproduced with permission from ref 72. Copyright 2021 MDPI. (c) Diagram showing the gradients observed in the OI. (d) Histological image of the osteochondral unit showing the different zones in the OI. The subfigure corresponds to a picrosirius red stained sample, imaged with a polarized light filter that shows the collagen distribution (aligned in orange and random in green). Panel d is reproduced with permission from ref 137. Copyright 2021 Elsevier. (e) Schematic of the ligament/tendon interface (enthesis, E) showing the predominant type of collagen and its orientation, and the type and morphology of the cells present in each zone. Panel e is reproduced with permission from ref 83. Copyright 2021 MDPI. (f) Diagram showing the gradients observed in the enthesis. (g) Histological image of the enthesis showing the different zones connecting the tendon and bone. The subfigure corresponds to a fluorescence microscope image showing the fibers of collagen type II in bright orange. Subfigure g is from ph.tum.de/latest/news/tendon-bone-insertion and reproduced with permission from ref 5. Copyright 2021 Nature.

even under normal physiological loading conditions.[10] These observations underline the importance of re-establishing the original properties of the native BSTIs for creating artificial biomimetic tissue interfaces.

Advances in tissue engineering offer promising solutions for repairing ruptured tissue interfaces through scaffold engineering and tissue grafting.[11,12] Engineered tissue scaffolds have mostly been manufactured through conventional technologies such as electrospinning,[13] freeze-drying,[14] salt leaching,[15] solvent-casting particulate leaching,[16] thermally induced phase separation,[17] gas foaming,[18] and emulsification.[19] Even though these fabrication techniques have shown remarkable progress, they are inadequate for accurately mimicking the hierarchical organization of native tissue interfaces.[20] The fabrication of monolithic biomaterials using conventional techniques challenges the inclusion of heterogeneous mechanical, chemical, and biological properties required for generating scaffolds to repair the degenerated interface.[21] Due to the intricacy of fabricating such scaffolds, recent approaches have shifted toward additive manufacturing (AM) technologies that focus on building 3D structures, also known as 3D printing. 3D printing includes very different approaches, such as vat photopolymerization, material extrusion, material jetting, binder jetting, powder bed fusion, direct energy deposition, and sheet lamination.[21−24] For language simplicity, the terms AM and 3D printing are used interchangeably in this review. AM technologies, and particularly multimaterial 3D printing, enable the fabrication of complex geometrical scaffolds with a high spatial resolution, as well as multiple gradients in 3-dimensions,[25−28] thereby potentially incorporating more than one material and other chemical and biological factors within a structure.[29] AM also offers an improved strategy to fabricate intricate multilayered and graded scaffolds with interconnected networks and porosities.

Although recently several complex multilayered and graded scaffolds have been developed to satisfy specific mechanical and biochemical cues for tissue interface engineering,[22,30−32] the challenge remains to reconstruct the interconnectivity of the bone-to-soft tissue to form the optimum interface that can maintain the structural integrity under different physiological loading scenarios. Previously published review articles have already described different techniques (*i.e.*, AM or non-AM) used for the fabrication of BSTIs.[6,7,21,33] Here, we discuss the limitations and challenges of those manufacturing techniques for fabricating various types of artificial interfaces. We also highlighted the current progress in extracting and implementing design motifs of natural interfaces (*e.g.*, interlocking mechanisms, functional gradient) into the design and fabrication of biomimetic interfaces which is essential for successful interface engineering. In this review, therefore, we aim to explore the current advances in the state-of-the-art design and fabrication of BSTIs. Toward this aim, we collected

https://doi.org/10.1021/acsbiomaterials.1c00620
ACS Biomater. Sci. Eng. 2023, 9, 3810−3831

some of the essential design principles and characteristics of the structure of BSTIs. We further identified the most important mechanisms mediating the load transfer in BSTIs, allowing deduction of biomimetic guidelines for tissue interface engineering.

2. CHARACTERISTICS OF BONE-TO-SOFT TISSUE INTERFACES (BSTIS)

Considering that bone-to-soft tissue replacements have to accurately mimic native tissue interfaces' functionality, it is crucial to understand how these interfaces are constructed and organized. A broad overview of three distinct BSTIs (*i.e.*, bone−cartilage, bone−tendon, and bone−ligament, Figure 1a) is provided in this section. The bone−cartilage interface is referred to as the osteochondral interface (OI), while the bone−tendon and bone−ligament interfaces are referred to as enthesis.

2.1. Osteochondral Interface (OI). The OI of synovial joints, such as the knee, consists of two distinct tissues, including the subchondral bone and articular cartilage. Cartilages serve to protect the subchondral bone, dissipate loads, and provide low-friction articulation of the joints.[34] Concurrently, articular cartilage consists of calcified cartilage and hyaline cartilage. The osteochondral tissues are specialized to withstand compressive forces with a (compressive) modulus of ∼1.8 MPa[35] in the articular cartilage and ∼3.7 GPa[36] in the subchondral bone.

The subchondral bone and the articular cartilage have their own explicit protein and extracellular matrix (ECM) organization and composition, resulting in multiple-level graded tissues with distinct functionalities. The subchondral bone is responsible for preserving the functional integrity of articular cartilage. The articular cartilage is in charge of transferring loads to the bone and distributing them over the articular surface. The noncalcified cartilage is separated from the subchondral bone by a layer of calcified cartilage. The interdigitated line between the noncalcified cartilage and the calcified tissue is called the tidemark, which is considered a calcification front.[37] The tidemark is not a straight line across the joint but a complex three-dimensional tissue structure (Figure 1b). The articular cartilage is integrated with the calcified tissues as a result of imbedding and interlocking forces that bind the cartilage to the subchondral bone plate. These forces are generated by collagen fibrils crossing from one layer to the other, producing a strong union between them.[38] The collagen junctions appear to have essential biological and biomechanical functions as they respond to microinjuries and transfer shear forces between layers,[39] which helps to reduce stress concentrations and improve tissue integration.[40,41] The biomechanical functionality of the OI relies on its native structure. Thus, the characterization of the native structure is critical for the successful development of a sustainable bone−cartilage interface.

The anatomy of the subchondral bone is highly variable in density, thickness, and composition. Bone tissue is primarily made of type-I collagen fibers mineralized by an inorganic ceramic compound called hydroxyapatite (HA), up to an extent of 85%.[42,43] The level of mineralization decreases to the calcified cartilage, having only 65% mineralization, and ultimately transfers to an uncalcified cartilage layer (Figure 1c).[43] The underlying bone is divided into two layers, namely the subchondral bone plate and the cancellous bone or subarticular *spongiosa*, confining the bone marrow.[44]

The subchondral bone plate consists of a dense cement line, known as the cortical end plate. The cement line represents a region of weakness.[45,46] When the cement line is viewed in a section perpendicular to the articular surface, it has the form of a solid mass fenestrated by several intercommunicating voids. The subchondral bone is comprised of plates that join together filling the intervening spaces when looking at it tangentially.[47] At the start of the cement line, these intervening spaces resemble honeycomb-like structures.[47]

Below the subchondral bone plate, the spaces enlarge and gradually elongate, forming mineralized lamellar sheets composed of parallel collagen type-I fibrils. Such sheets are oriented perpendicular to the articular surface and form a trabecular structure, known as the cancellous bone (Figure 1d).[47] Based on the architecture, there are three types of cancellous bone. Type I consists of a very delicate meshwork of fine rod-like trabeculae. This meshwork is widely distributed and is typically seen in the deeper parts of the end of long bones. Type II consists of both rod- and plate-like trabeculae and is generally found at the end of long bones (subtype IIa), in the calcaneum (subtype IIb), and at the lower end of the femur (subtype IIc). Type III is entirely made up of platelike trabeculae, forming a meshwork with or without the presence of a directional orientation.[47] Thin delicate plates form subtype IIIa, whereas larger plates enclosing tubular spaces form subtype IIIb. In the areas where cancellous bone is very dense, the platelets are relatively small and thick enclosing irregular spaces. These spaces have a honeycomb-like appearance when spaces are small but show a directional orientation when the spaces are larger (Figure 1d).[47] Differences in the trabecular structure are related to distinct mechanical properties for weight and nonweight bearing areas in the bone.[44]

The noncalcified cartilage is divided into three layers including superficial, middle, and deep zone (Figure 1b−d), which share the basic cartilage framework made from fibrillary type II collagen copolymerized with type XI and IX collagens[48,49] and aggrecan[50,51] as the main proteoglycan. The aggrecan core protein has glycosaminoglycans (GAGs). Attached GAGs are the glycoproteins responsible for maintaining water homeostasis and osmolarity, providing cartilage its shock-absorbing capabilities. The size, structure, and orientation of collagen fibers and chondrocytes (cells present in cartilage) vary in a graded manner within articular cartilage. In the superficial zone, collagen fibers and chondrocytes are laid parallel to the surface. The middle zone is characterized by the random alignment of collagen fibers.[52] A denser collagen network and the chondrocytes perpendicular to the articular surface can be found in the deep zone. The density of chondrocytes is higher in the superficial zone, whereas they are more dispersedly arranged in the deep-radial and transition zones.[41] For instance, the gradient in chondrocyte density per region varies from 7.000 to 24.000 cells/mm^3 in the articular cartilage of the femoral head in adult human knee joints.[41]

The gradient in the mineralization levels, collagen fiber composition and alignment, and chondrocytes' orientation and distribution result in a gradually changing stiffness over the different regions of the osteochondral interface (Figure 1b−d), allowing for an effective force absorption during contact.[53]

2.2. Enthesis. Bone−tendon and bone−ligament interfaces are represented by the enthesis. Tendons attach muscles to bones, allowing for movement of the body by transferring muscle forces while ligaments attach two bones together and

https://doi.org/10.1021/acsbiomaterials.1c00620
ACS Biomater. Sci. Eng. 2023, 9, 3810−3831

provide passive stability to the joints.[54] The enthesis tissues are specialized to withstand tensile forces with the elastic moduli of ∼0.45 GPa in the tendon,[5] ∼17−21 GPa in the cortical bone,[55,56] and ∼0.35−2 GPa in the trabecular bone.[56,57] In contrast to cartilage, tendons and ligaments are built to withstand tensile forces, provided that they consist of tough bands of fibrous tissues.

Entheses are highly anisotropic structures, organized in a graded manner ranging from tendon or ligament to bones over a relatively small transition length. In humans, the length scale of the interface region can range from 100 μm to 1 mm, depending on the age, specific function, and placement of the enthesis.[5,7] Two different types of entheses can be distinguished in the human body, a fibrous and a fibrocartilaginous enthesis.[58−61] In a fibrous enthesis, collagen fibers known as Sharpey's fibers intrude the bone forming acute angles.[62] The fibers embed into bone via the periosteum, providing a firmer hold for short ligaments and tendons.[63] This type of enthesis is found, for example, between the periodontal ligament and the alveolar bone, which is the thickened bone at the socket of teeth.[63] The fibrocartilaginous enthesis is more common and can be found in regions that connect two bones through a ligament, *e.g.*, the anterior cruciate ligament (ACL),[64] or connect tendons to bone, *e.g.*, the supraspinatus tendon of the rotator cuff muscles.[65]

The enthesis transitions in composition and structure from one tissue to another (Figure 1e−g). This transition consists of a heterogeneous distribution of cell types, such as osteoblast and tenocytes, secreting specialized extracellular matrices. These matrices contain distinct biochemical and biophysical compositions, resulting in different mechanical properties.[64,66] The enthesis can be divided into four regions, *i.e.*, the ligament or tendon, uncalcified fibrocartilage, calcified fibrocartilage, and bone as schematically illustrated in Figure 1e. Tendons and ligaments are connective tissues made of type-I collagen fibers arranged as a network of densely aligned collagen fibrils.[40] This region of the enthesis is similar to the midtendon or -ligament and has comparable mechanical properties. It is populated by fibroblasts embedded along the linearly arranged fibrils and extends into the subsequent uncalcified fibrocartilage.[40,65]

The uncalcified fibrocartilage is an avascular zone of unmineralized fibrocartilage that contains ovoid-shaped fibrochondrocytes as shown in Figure 1e.[40] The ECM is made of collagen type-I, -II, and -III fibers and includes proteoglycans. This uncalcified region is crucial for the normal functioning of the enthesis as it acts as a force damper.[65] It dissipates bending forces generated by the narrowing of the tendon or ligament and transfers forces away from the enthesis. In the enthesis, the tidemark is a basophilic line that divides the calcified and uncalcified fibrocartilage regions, forming a mechanical boundary between soft (unmineralized) and hard (mineralized) tissues.[65,67]

The calcified fibrocartilage is predominantly made of mineralized collagen type-II fibers, as well as some type-I and proteoglycans. This region is also characterized by the presence of collagen type X and is populated by fibrochondrocytes. In contrast to the smooth transition between uncalcified and calcified fibrocartilage, the bone's calcified fibrocartilage attachment is highly irregular (Figure 1g).[65] The irregular interface increases the structure's integrity as it improves the mechanical interlocking mechanism through interdigitation.[67,68] It was previously proposed that the depth and frequency of interdigitation are related to the bonding strength of tendons and ligaments to bone.[69,70] Interdigitation increases the area over which forces are transduced, reducing stress concentrations and making the interface more resilient and durable.[5] Bone is predominantly made of mineralized type-I collagen fibers and provides a solid attachment site for tendons and ligaments.[65]

Collagen type I fibers in the tendon appear to unravel into thinner fibers just before entering the bone. These more delicate fibers splay outward rather symmetrically in angles of ∼15° with respect to the tendon fibers.[5] This results in the previously discussed interdigitated line, where groups of fibers together interlock with bone (Figure 1g). Further detection with a laser deflection signal has shown that these thinner fibers are located in the transition zone (*i.e.*, the zone between the uncalcified and calcified fibrocartilage) and coincide with collagen type-II fibers forming network-like fiber arrangements.[5] The combination of these elements leads to formation of a transition zone that is more compliant than both tendon and bone. The overall compliance of this region is ten times higher than the remaining tendon and occurs in the area where fiber subdivision and outward splaying are observed.[5] Altogether, the enthesis is highly adapted to transfer tensile forces over a micrometer length scale.[5−7]

3. SCAFFOLD ENGINEERING FOR BONE-TO-SOFT TISSUE INTERFACES

Nature has provided various solutions for joining dissimilar biological materials utilizing gradients in the biomineralization process [66], as can be seen, for example, in musculoskeletal interfaces of human and animal bodies combining mineralized (e.g., bone) and soft tissues (*e.g.*, ligament and tendon interfaces).[41,65] Some more examples of mineralized tissues are teeth,[71] fish scales,[33] seashells,[33] mussel byssal threads,[1] and polychaeta jaws,[1] which are all made of different layers of materials that have various degrees of mineralization. The hard and stiff biominerals are located in regions experiencing high mechanical stresses and abrasion. These biological hard−soft connections have proven effective in transitioning between materials with large dissimilar properties.[33] Therefore, adopting biomimetic strategies can help to advance the field of tissue interface engineering.

In addition to the spatially controlled material strategy to fabricate bone-to-soft scaffolds, it is important to consider the different (cell) organizations[72] shown in each tissue. Nature has adopted anisotropic structures (Figure 1b−g) for specialized load-bearing functions. For instance, the transition from tendon's crimped to aligned collagen bundles is the optimized design strategy offered by Nature to introduce anisotropic material properties for this tissue. This helps tendons to support high tensile loads in the direction of fiber alignment.[73] In articular cartilage, the arcade-like collagen organization helps to dissipate high loads passing through human joints.[74]

3.1. Biomimetic Strategies. Each natural hard−soft interface has its own distinct properties that come from variations in chemical compositions and microstructural geometries. The specific factors that influence the chemical composition of biomaterials are mineralization, inorganic ions, biomolecules, and hydration levels. The microstructural properties are, however, influenced by the arrangement, distribution, dimension, and orientation of components in the tissue. These factors are spatially adjusted from nano- to near macroscales.[33] The spatial variation of these factors

https://doi.org/10.1021/acsbiomaterials.1c00620
ACS Biomater. Sci. Eng. 2023, 9, 3810−3831

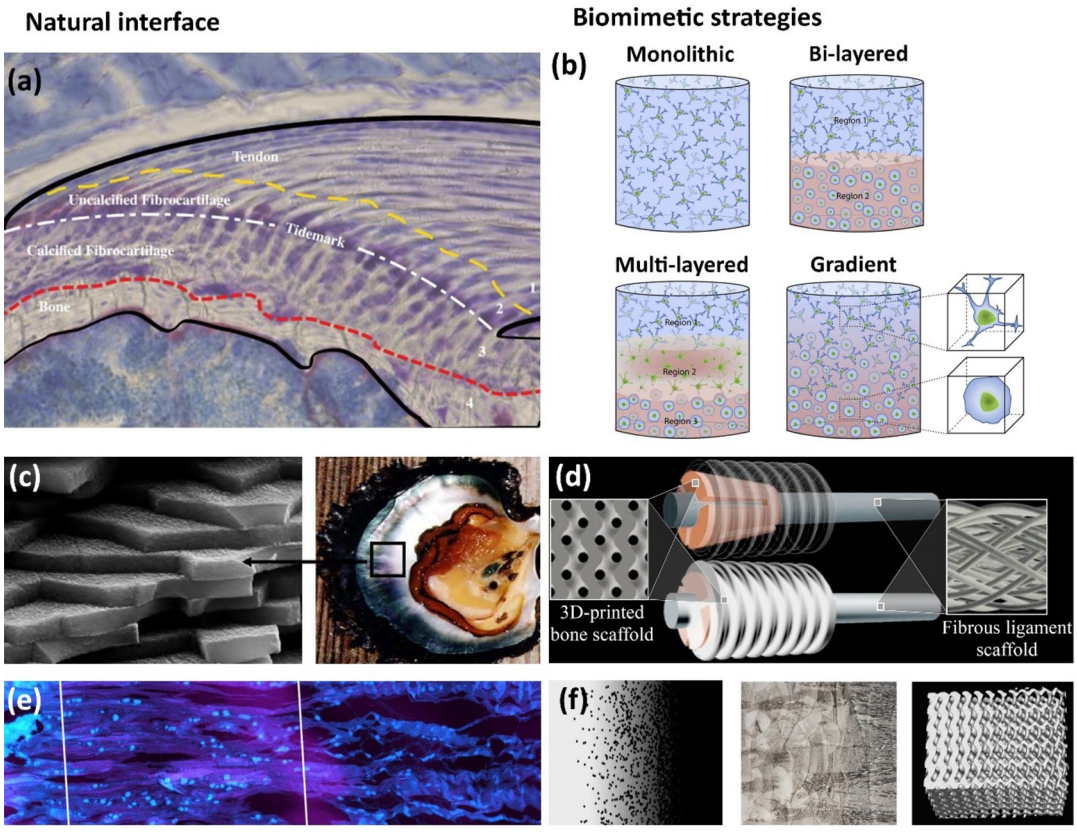

Figure 2. (a) Histological illustration of the enthesis of a mouse supraspinatus, consisting of four zones: bone, calcified fibrocartilage, uncalcified fibrocartilage, tendon. Panel a is reproduced with permission from ref 65. Copyright 2021 Muscle, Ligaments and Tendons Journal. (b) Biomimetic strategies for hard−soft interface tissue engineering, including the use of monolithic, layered, and gradient scaffolds with different cell types and materials properties resembling the native tissue. Panel b is reproduced with permission from ref 21. Copyright 2021 Elsevier. (c) Brick-and-mortar structure of nacre. Copyright 2021, M. Rousseau. Originally published in ref 101 under CC BY 3.0 license. Available from DOI: 10.5772/22978. (d) Illustration of a complex bone screw biomimetic design comprised of 3D-printed porous bone and fibrous scaffolds aiming at regenerating the bone−soft tissue interface. Panel d is reproduced with permission from ref 143. Copyright 2021 Elsevier. (e) Cryo-cut cross section of the porcine bone−tendon interface, displaying dense morphology to fibrous-like structure (from left to right). Panel e is reproduced with permission from ref 61. Copyright 2021 PLOS. (f) Biomimetic approaches for the hard−soft interface using functionally graded design by varying the composition (left), microstructure (middle), and porosity (right). Panel f is reproduced with permission from ref 104. Copyright 2021 MDPI.

creates a gradual change in material properties that can help bridge the transition between dissimilar materials. These incremental changes minimize the interfacial stresses by creating a "fuzzy" boundary (Figure 2a), avoiding abrupt changes in mechanical properties.[1] By alleviating the interfacial regions of stress concentrations, the mechanical performance of hard−soft interfaces improves. The fabrication of graded materials containing a "fuzzy" boundary has only recently taken root.[33]

A secondary biomimetic strategy is to increase the energy of adherents along the contact surface of dissimilar materials.[1] Mussels, for example, produce proteins in their holdfasts, which makes it possible to generate strong and long-lasting adhesive bonds under hostile conditions onto hard rocks, metals, or glasses.[75] These adhesive bonds are formed by modified amino acids, which form charge-transfer chelate complexes with oxides on the opposing surfaces.[76] Most adhesives work through the formation of covalent bonds, but they can also form ionic or static (attractive) bonds between surface atoms and adhesive constituents.[77] These bonds are the chemical links that transfer loads from surface to surface.[77] Adhesives have been used in the form of surface coupling treatments or "primers" for a long time. A surface coupling treatment increases or changes the tension, roughness, or chemistry of the surface, thereby improving the strength and durability of the joint.[77] A primer is usually a diluted solution of an adhesive in an organic solvent that is specifically made to match the materials.[78] By priming the surface between two materials, adhesive bonds can form between highly dissimilar materials such as metals and polymers.[1]

A third strategy found in Nature is the presence of a compliant zone between hard and soft phases. An example is the transition zone of the enthesis, where the compliance of this region is at least ten times that of tendon or bone.[5] This result may seem odd as it further increases the mismatch in stiffness between the tissues. Yet, it has been shown that when two elastic wedges with dissimilar material properties are orthogonally bonded together and undergo normal and shear stresses, the generated edge-stress singularities depend on not only the mismatch in elastic moduli but also their Poisson ratios and shear moduli.[79] This corresponds with the study by Liu et al. (2012), which has shown through numerical optimizations how a compliant zone between tendon and bone reduces stress concentrations at the attachment site of an idealized mathematical model of the rotator cuff.[80] It has been proposed that by increasing local deformation in the compliant zone, this zone is able to act as an energy-absorbing component and thereby helps to maintain the structural

https://doi.org/10.1021/acsbiomaterials.1c00620
ACS Biomater. Sci. Eng. 2023, 9, 3810−3831

integrity of the interface.[81] This phenomenon appears to be relatively common in Nature, as it is observed in the enthesis,[5,80−83] the anchoring of teeth,[84] and marine mussels attachment to hard surfaces.[85] Altogether, these strategies can be used to infer biomimetic guidelines for tissue interface engineering.

3.1.1. Geometrical Designs. Designing a resilient and durable connection at the hard−soft interface is worth exploring the geometry of mechanical interlocking designs found in Nature. Generally, mineralized tissues, such as bone, tooth, and nacre, contain a large number of interfaces between stiff and compliant components at different length scales.[86] The mechanical performance of these biological composites critically depends on the mechanical properties of the interfaces. To strengthen the interface, Nature adopts a hierarchical strategy observed as interfacial roughness on different length scales.[5,68,87,88] This can be regarded as the interdigitated line between tendon and bone on a micrometer length scale[5] and as interfacial nanoasperities on aragonite tablets on a nanometer length scale.[88] Interfacial roughness increases the contact area between stiff and compliant constituents, resulting in a higher magnitude of plastic strains after yield.[86] The study by Launey et al. (2009) showed that surface roughness on a ceramic−polymer interface plays a critical role in controlling shear forces during loading. It increases the sliding interference of the interface and thereby enhances energy dissipation efficiency.[89]

Similar hierarchical systems inspired by Nature are fractal patterns, consisting of identical repeating geometries.[90] For example, cranial sutures on mammalian skulls,[91] and sutures on the shell of Ammonoids,[92] use hierarchical fractal patterns to optimize their mechanical properties. Inspired by such structures, Zhang et al. (2012) used finite element models to show that geometrical interlocking designs with additive fractal patterns have a significantly higher interfacial strength than nonfractal interlocking designs.[86] The interfacial strength increases due to a more homogeneous stress distribution in the compliant zone. A similar study investigated the effect of hierarchical fractal modes on the resulting strength, stiffness, and failure modes of triangular interlocking designs. It showed that increasing the structural hierarchy improved the load resistance of the interlocking designs and prevented premature failure of the interfaces.[93] One of the effective design strategies to improve the mechanical properties of the interface with limited material options is to use structural hierarchy in suture joints.[93]

Another important factor influencing the interfacial strength of suture joints is the large-scale geometry of the interlocking design. The study by Zhang et al. (2012) showed that a sawtooth pattern (triangular-based geometry) has a higher interfacial strength than an antitrapezoidal pattern.[86] Accordingly, other studies examined the effects of alternative geometries on the resulting interfacial strength and stress distribution of composite structures under load.[93−97] For instance, the mechanical behavior of triangular and rectangular suture joints connecting stiff components through a compliant interfacial seam was examined in ref 94. This study formulated quantitative analytical and computational models to predict the strength, stiffness, and stress distribution of different models. The mechanical properties of these models can be used to evaluate variations in the deformation and failure mechanisms of different geometrical patterns. Their analyses showed that triangular suture joints significantly outperform rectangular suture joints by having a maximum strength twice as large.[94] The researchers attribute this finding to a more homogeneous stress distribution throughout the entire structure, which corresponds to the observations reported in ref 86. The study also showed that high levels of shear resistance at the interface enable higher levels of interfacial strength, corresponding to the hypothesis that interfacial surface roughness increases sliding interference and thereby enhances the efficiency of energy dissipation during loading.[89]

The deformation mechanics and failure modes of trapezoidal, antitrapezoidal, rectangular, and triangular interlocking were investigated in ref 95. The mechanical properties of such mechanical interlocking interfaces were shown to be affected by several geometric parameters, such as the tip angle of a triangular geometry or the wavelength and tooth shape of a trapezoidal geometry.[95] Triangular geometries possess the highest stiffness and strength, due to their ability to distribute stresses uniformly throughout the entire structure.[95] Antitrapezoidal geometries are more desirable for their toughness and damage tolerance, resulting from an increased strain to failure and an improved mechanical interlocking mechanism.[95] The damage tolerance is an important parameter for biological materials, because it keeps the surfaces close to each other, providing them the ability to regenerate.[95] The geometrical patterns and their parameters should be tailored and fine-tuned to optimize the performance of these suture interfaces under specific loading conditions.[95−97]

3.1.2. Functionally Graded Materials. Functional gradients form a distinctive feature of natural hard−soft interfaces (Figure 2a−e). The advantage of functional gradients is that a gradual compositional change (*e.g.*, degree of mineralization) reduces the stress concentrations at the interface. This has led to the development of functionally graded materials (FGMs) (see Figure 2b), with promising features for emerging material applications. FGMs are composites fabricated from two or more components. There are many potential applications, including but not limited to the automotive, electronic, telecommunication, aerospace, defense, and biomedical industries.[98−100]

In Nature, the building blocks of graded structures primarily are created using the occurrence of (hard) inorganic and (soft) organic components.[2] These building blocks allow the opportunity to gradually change the material properties and integrate specific mechanisms into a structure. An example of such a mechanism is a brick-and-mortar structure found in the nacre (Figure 2c), which serves to toughen the material.[101,102] This specific structure hinders the propagation of subcritical cracks due to a periodically varying elastic modulus.[89,102]

The inherent multicomponent nature of FGMs makes it possible to replicate such structures, providing the opportunity to create materials with tailor-made properties. For example, high strength and toughness are mutually exclusive properties in engineered materials.[103] Metals are examples of tough, while ceramics are examples of strong, stiff materials. This makes certain materials predestinated for a particular set of applications. However, the formation of FGMs provides the possibility to combine these opposing material properties in one structure. This means the stiff ceramic particles can be compensated by tough metallic ones.[98] This results in a material with more favorable elastic-plastic behavior. It has been shown that functionally graded implants from combined metallic and ceramic particles have a longer life span and perform better than full metallic implants.[104]

https://doi.org/10.1021/acsbiomaterials.1c00620
ACS Biomater. Sci. Eng. 2023, 9, 3810−3831

Table 1. Synthetic Bone-Cartilage Scaffolds Manufactured Using Various Techniques and Biomaterials[a]

Study	Materials for bone	Materials for cartilage	Scaffold design	Fabrication methods	Mechanical properties (compressive)	Biological aspect
24	PCL with SAPH	PCL with SAPH	Monolithic	AM (FDM)		*In vivo* study for 3% SAPH-coated PCL-scaffold showed cell proliferation and osteogenic differentiation.
17	PLGA with nano-HA	PLGA with nano-HA	Monolithic	Thermally induced phase separation, annealing and freeze-drying	EM: 0.55 MPa	Higher viability and proliferation of MSCs as compared to PLGA suggested potential use for the cartilage repair in clinical application.
177	Agarose hydrogel with HA	Agarose hydrogel with HA	Monolithic	Casting	EM: 4.3 kPa Shear modulus: 8.7 kPa	Hydrogel-ceramic composite was cultured using chondrocytes that showed optimal mineral aggregate size and content of the native tissue interface.
23	Chitosan-Gelatin-HAc with GR	Chitosan-Gelatin-HAc	Monolithic (Two types)	3Dbioprinting	EM 0.06% GR: 8 MPa EM 0% GR: 4 MPa	Biocompatibility test under interaction with P3 BMSC.
120	PLGA with nano-HA	PLGA	Bilayered	Casting and sintering	Bony-layer EM: 142 MPa Cartilage-layer EM: 62 MPa Combined EM: 85 MPa	High cell viability for the cell analysis with rabbit chondrocytes and BMSCs.
121	PLGA-PEG foam	PGA-nonwoven mesh	Bilayered			Seeding each layer of PLGA-PEG foam and PGA separately with periosteal cell and chondrocyte for 1-week (immature) as compared to 4-week (mature) construct demonstrated better cartilage/bone integration.
115	PCL with HA	PGA/PLA	Bilayered	AM-FDM	Bony-layer EM: 58 MPa Cartilage-layer EM: 5 MPa	Successful femoral head tissue regeneration of mice.
116	PCL with PDO-nanospheres	PEG-hydrogel with PLGA-nano-spheres	Bilayered	Casting and UV-light irradiating	Bony-layer EM: 22 MPa Cartilage-layer EM: 6 MPa	Improved human MSC adhesion in differentiation to the artificial layers as compared to pure PCL-scaffold.
118	PLA with G5 bio-glass	PLA	Bilayered	AM	Bony-layer EM: 44 MPa Cartilage-layer EM: 28 MPa	Addition of G5 bioglass lead to a higher vascularization of the implant and consequently promoted bone regeneration.
170	PVA-NOCC (hydrogel) with HA	PVA-NOCC (hydrogel)	Bilayered	Tissue harvesting, casting and freezing		*In vivo* biocompatibility test using of a rat model showed that the bilayered construct may have a promising potential for osteochondral defect.
171	HA with polyamide6	PVA	Bilayered	Freezing-thawing and high-temperature annealing		The evaluation of bilayered scaffolds for biocompatibility, osteogenesis and chondrogenesis using ectopic osteochondral construct showed potentials for *in situ* osteochondral defect repair.
172	polyHEMA(38)-hydrogel with HA	polyHEMA(200)-hydrogel with HAc	Bilayered	Sphere-templating and freeze-drying	Dry EM: 39 MPa Wet EM: 0.09 MPa	Cyto-compatibility test with human MSCs and chondrocytes
178	Plasmid BMP-2-activated chitosan-gelatin with HA	Plasmid TGF-β1-activated chitosan-gelatin	Bilayered	Casting, salt-leaching and freeze-drying		Spatially controlled and localized gene-activated bilayered scaffold showed significant cell proliferation and induced cell differentiation for *in vitro* results of the rabbit knee osteochondral defect model.
15	Silk fibroin with CaP	Silk fibroin	Bilayered	Salt-leaching and freeze-drying	EM: 0.4 MPa	*In vitro* tests of rabit bone MSCs supported cell attachment, viability and proliferation in interaction with the scaffold.
138	Agar scaffold	PEGDA with HA	Bilayered	Casting and UV-light irradiating	EM: 145 kPa Shear strength: 5.9 kPa	The presence of HA increased interfacial shear strength of the scaffold as early as 7 days of *in vitro* tissue culture enhancing the integration of engineered cartilage to bone.
30	PLGA microsphere scaffold	Alginate hydrogel	Multilayered (3 layers)	Sintering and freeze−thawing	EM: 7.8 MPa	The multiphasic scaffold exhibited superior tissue repair efficacy in a rabbit knee defect model with a gradient transition and integration between cartilage-bone tissue. However, after decellularization the tissue repair efficacy of the graft decreased, remaining challenges for the industrialization of the graft.
14	Deep zone: Collagen type-I with HA	Intermediate zone: Collagen type-I and II with HA Superficial zone: Collagen type-II with HAc	Multilayered (3 layers)	Freeze-drying		The Scaffold in a critical-sized defect was tested *in vivo* in a rabbit knee. The results showed that it was able to guide the host reparative response leading to tissue regeneration with a distinct zonal organization.
173	Silk fibroin with HA	Silk fibroin	Multilayered (3 layers)	Paraffin-sphere leaching and thermally induced phase separation	Bony-layer EM: 55−110 kPa Cartilage-layer EM: 52−84 kPa	Good biocompatibility results of the multiphasic scaffold supported cell growth and differentiations toward chondrocytes and osteoblasts. Particularly, it showed that the intermediate layer can play a role in preventing mixing cells with each other within the chondral and the bony layers.

https://doi.org/10.1021/acsbiomaterials.1c00620
ACS Biomater. Sci. Eng. 2023, 9, 3810−3831

Table 1. continued

Study	Materials for bone	Materials for cartilage	Scaffold design	Fabrication methods	Mechanical properties (compressive)	Biological aspect
174	Chitosan with HA	Chitosan-Silk fibroin	Multilayered (4 layers)	Temperature gradient processing	Full scaffold EM: 150 kPa Bone-layer EM: 260 kPa	14 days cell culture showed that the scaffolds were able to well support the growth and infiltration of cells, suggesting a promising potential for articular cartilage repair.
117	PCL-β-TPC composite	PCL	Gradient	Hybrid extrusion and electrospinning	Only tensile tests, no compressive tests. EM: 18.5−27.5 kPa UTS: 810−1080 kPa	The graded scaffold showed better distributions of various biological factors, including the concentrations of drugs/growth factors, and biodegradation rate required for fabricating complexity of the native tissue.
180	GelMA-GG-hydrogel with HA	GelMA-GG-hydrogel	Gradient	Casting and freeze-drying		The cell culture results of the graded scaffold showed an upregulation of the prevasculature formation in the bone-like region while it was downregulated in the cartilage-like region.
22	PNAGA-hydrogel with monomer	PNAGA-hydrogel	Gradient	AM (bioprinting)	EM compressive: 20−137 kPa EM tensile: 20−43 kPa Max. tensile strength: 0.41 MPa Max. compressive strength: 137 MPa	The *in vivo* animal evaluation of biohybrid gradient hydrogel scaffold showed simultaneous regeneration of both cartilage and subchondral bone within osteochondral defects.
179	PACG-GelMA-hydrogel with bioactive glass	PACG-GelMA-hydrogel with Mn^{2+}	Gradient	AM (bioprinting)	EM compressive: 837 kPa EM tensile: 320 kPa Max. tensile strength: 1.1 MPa Max. compressive strength: 12.4 MPa	*In vitro* biological experiment and *in vivo* implantation showed that the biohybrid gradient hydrogel scaffold can facilitate the concurrent regeneration of subchondral bone and cartilage in a rat model.
182	Collagen with HA	Collagen	Gradient	Casting and diffusion		

[a]The acronyms summarized in this table are PCL = polycaprolactone, SAPH = self-assembling peptide hydrogel, FDM = fused deposition modeling, PLGA = poly(lactide-*co*-glycolide) acid, HA = hydroxyapatite, EM = elastic modulus, HAc = hyaluronic acid, GR = graphene, PEG = polyethylene glycol, PGA = polyglycolic acid, PDO = poly(dioxanone), PLA = polylactic acid, UV = ultraviolet, PVA = poly vinyl alcohol, NOCC = N,O-carboxymethylated chitosan, HEMA = hydroxyethyl methacrylate, PEGDA = poly(ethylene glycol) diacrylate, CaP = calcium phosphate, TCP = tricalcium phosphate, GelMA = methacrylated gelatin, GG = gellan gum, PNAGA = poly(*N*-acryloyl glycinamide), PACG = poly(*N*-acryloyl 2-glycine), Mn^{2+} = manganese ions, FDM = fused deposition modeling, MSCs = mesenchymal stem cells, BMSCs = bone marrow stem cells.

The components of FGMs vary spatially to optimize the material properties for specific functions.[98] Manufacturers can use continuous as well as discrete functions to change the components gradually. While continuously graded functions usually resemble a linear or sigmoid design, discrete graded functions normally vary the frequency and magnitude of the steps.[2] FGMs can be divided into three different groups (*i.e.*, the gradient in composition, microstructure, or porosity (Figure 2d and f).[104] Each gradient can serve a distinct purpose depending on the desired mechanical performance of the material.

3.2. Biomaterials. The selection criteria for biomaterials in orthopedic implants depend highly on the type of tissue and the function of the implant. It is important to understand the underlying tissues and their loading conditions in order to determine the biomaterials that fit specific parts of the BSTIs.

Here, we divided biomaterials into two main groups. Hard materials refer to materials representing the mechanical properties of hard tissues (*i.e.*, bone), while soft materials refer to those representing the properties of soft tissues (*i.e.*, cartilage, tendon, and ligament).

3.2.1. Hard. The materials used for orthopedic bone implants are primarily metallic, as they form load-bearing structures requiring a high mechanical reliability. Prominent biocompatible metals are titanium-based alloys, cobalt−chromium-based alloys, and stainless steel.[42] A disadvantage of metallic materials is their high density and stiffness,[104] causing stress shielding and subsequent bone remodeling.[105] This has contributed to the exploration of other materials (*e.g.*, ceramics and synthetic polymers).

Ceramics have been proven to possess desirable properties such as good inert behavior, high strength, and minimal thermal and electrical conductivity for hard tissue replacements. The disadvantages of ceramics are the low ductility and high brittleness of the materials.[106] Nevertheless, ceramics have played a substantial role as a biomaterial for orthopedic implants. Primarily bioactive ceramics are defined as ceramics that bond directly with bone without the need for connective tissue engagement.[107] The most common bioceramics include

https://doi.org/10.1021/acsbiomaterials.1c00620
ACS Biomater. Sci. Eng. 2023, 9, 3810−3831

Table 2. Synthetic Bone−Tendon Scaffolds Manufactured Using Various Techniques and Biomaterials[a]

Study	Material bone	Material tendon	Scaffold Type	Processing method	Mechanical properties (tensile)	Biological aspect
199	PLGA-nanofibers with HA	PLGA-nanofibers	Monolithic (two types)	Electrospinning		
209	Random PLGA-nanofibers	Aligned PLGA-nanofibers	Monolithic (two types)	Electrospinning and rotating mandrel electrospinning	Random scaffold EM: 107 MPa YS: 2.5 MPa UTS: 3.7 MPa Aligned scaffold EM: 341 MPa YS: 9.8 MPa UTS: 12 MPa	The organization and arrangement of nanofibers significantly affect the human rotator cuff fibroblast responses including cell attachment and matrix deposition. This controlled cell response exhibited potentials for tendon regeneration.
210	Random PLGA-nanofibers	Aligned PLGA-nanofibers	Bilayered	Electrospinning	Aligned EM: 143 ± 98 MPa Random EM: 53 ± 24 MPa	Culturing tendon cells on scaffolds with aligned and random nanofiber orientation showed respectively random and aligned cell orientation.
32	PCL-microfibers with PLGA-microspheres	PCL-microfibers with PLGA-microspheres	Multilayered (3 layers)	AM	Stiffness: 15 N/mm Max load: 20 N	The engineered multiphase fibrocartilaginous interface scaffold was tested *in vitro* using mesenchymal progenitor cells and *in vivo* as it was implanted at the bone−tendon interface in a rat rotator cuff repair model. The scaffolds successfully promoted the regional differentiation, consequently leading to enhanced healing of bone−tendon interfaces.
214	Collagen-GAG and CaP	Collagen-GAG interface zone: PEG-hydrogel	Multilayered (3 layers)	Freeze-drying (+ diffusion and gelation)	Storage modulus G′eq: between 4 and 16 kPa	
201	Collagen and HA	1. Collagen 2. Cross-linked aggrecan-collagen (chondroitin sulfate) 3. Partly calcified collagen	Multilayered (4 layers)	Freeze-drying	EM (1,2,3,4): 0.3/1.2/3.0/4.5 MPa Elongation at breakpoint: 113%/106%/82%/71%	The *in vitro* results of the multilayer scaffold supported the adhesion and proliferation of human fibroblasts, chondrocytes, and osteoblasts.
196	PLGA-nanofibers with CaP	PLGA-nanofibers	Gradient	Electrospinning and plasma treatment		The level of mineral content on the surface of the nanofibers can control the osteogenesis of ASCs for enthesis repair.
200	PLGA-nanofibers with HA	PLGA-nanofibers	Gradient	Electrospinning	EM: 3.1 GPa	
13	PLGA/PCL-Gelatin-nanofibers with CaP	PLGA/PCL-Gelatin-nanofibers	Gradient	Electrospinning	EM: 40−120 MPa	Introducing gradient in the calcium phosphate content has influenced the activity of mouse preosteoblast MC3T3 cells.
211	Random PCL-nanofibers	Aligned PCL-nanofibers	Gradient	Electrospinning		The scaffolds were seeded by ASCs which exhibited different morphologies at different locations. These results were because of the capability of the fabrication technique in encapsulation of desired materials inside deposited nanofibers.
197	Random PCL-nanofibers	Aligned PCL-nanofibers	Gradient	Electrospinning		The random-to-aligned interface scaffolds were cocultured by osteosarcoma and fibroblast cells which resulted in a random-to-aligned cocultured tissue interface after 96 h culturing mimicking the microarchitecture of enthesis.
31	PCL-Gelatin-microfibers with HA	PCL-Gelatin-microfibers	Gradient	Wet-spinning and knitting	PCL/gelatin EM: 252 MPa YS: 4.7 MPa Strain to failure: 295% PCL/gelatin/HA EM: 59 MPa YS: 1.0 MPa Strain to failure: 442%	The results of biological performance using human ASCs showed that topography of PCL/gelatin microfibers can induce cellular anisotropic alignment (*i.e.*, cytoskeleton elongation), resembling native tenogenic organization.
66	PUR-QHM-polymers (UV-exposed)	PUR-QHM-polymers	Gradient	Photocross-linking, and heat-curing	Tensile tests EM: 0.6−2.7 GPa YS: 12−74 MPa Compressive tests	Biophysiochemical results showed favorable characteristics for bone−tendon repair.

https://doi.org/10.1021/acsbiomaterials.1c00620
ACS Biomater. Sci. Eng. 2023, 9, 3810−3831

Table 2. continued

Study	Material bone	Material tendon	Scaffold Type	Processing method	Mechanical properties (tensile)	Biological aspect
					EM: 1.5− 3.0 GPa YS: 58−121 MPa	

[a]The acronyms summarized in this table are PLGA = poly(lactide-*co*-glycolide) acid, HA = hydroxyapatite, PCL = polycaprolactone, EM = elastic modulus, YS = yield strength, UTS = ultimate tensile strength, GAG = glycosaminoglycan, CaP = calcium phosphate, PUR = polyurethane, QHM = Quadrol hexamethylene diisocyante, UV = ultraviolet, adipose-derived mesenchymal stem cells = ASCs.

bioactive glass and calcium phosphate ceramics (CaP).[21,107] Bioactive glasses belong to a group of surface reactive glass−ceramic composites made of different percentages of SiO_2, Na_2O, CaO, and P_2O_5, synthesized by a melt or sol−gel process to create interconnected pore networks.[108] The most famous and the original bioactive glass is Bioglass. It has been used in many bone implants, such as cranial defects or mandibular traumas, due to its high osteoinductivity.[108−110] The calcium phosphate (CaP) ceramics are one of the most studied materials for bone tissue engineering that include tricalcium phosphate (TCP, either α or β), tetracalcium phosphate (TTCP), octacalcium phosphate (OCP), and $Ca_{10}(PO_4)_6(OH)_2$, which is better known as hydroxyapatite (HA).[111] The rationale for using calcium phosphate derived ceramics, such as HA, is that they are found naturally in the body, and they show important characteristics such as biocompatibility, osteoconductivity, and biodegradability.[112] In addition, HA can be combined with other materials, such as collagen scaffolds, to improve its use in AM. These composites are described in more detail elsewhere.[113]

Synthetic polymers have been widely used as another class of biomaterials for both bone and soft tissue replacement purposes. This is because their properties can be tuned in such a way to cover a broader range of mechanical properties. This can be done by changing their molecular weight, level of cross-linking, and crystallinity through adding certain material mixtures.[114] Their mechanical properties also depend on the fabrication methods (see section 3.3). For instance, the polymeric materials polycaprolactone (PCL)[24,115−117] and polylactic acid (PLA)[118] are frequently used materials for bone scaffolds. PCL is a biodegradable and biocompatible polymer with tough nylon-like properties that softens at low melting points.[119] The PCL-scaffolds have a relatively high mechanical strength in comparison to other scaffolds. Their elastic moduli range between 5 and 58 MPa,[115,116] depending on their fabrication method and material mixture. However, the structural characteristics of the PCL-molecule make it hydrophobic, thereby making it challenging to culture cells on PCL-scaffolds.[24]

As another example, poly(lactic-*co*-glycolic acid) (PLGA) has been a popular polymer for the fabrication of bone and cartilage-like scaffolds,[30] making it a natural successor for osteochondral scaffolds.[17,30,120,121] PLGA is a highly biocompatible polymer with tunable degradation rates and FDA-approval.[30,122] This polymer has been shown to promote cell adhesion and have favorable mechanical properties, as shown in Table 1, for bone- and cartilage-like tissues.[123] A comprehensive list of polymeric materials used for bone scaffolds can be found elsewhere.[124]

3.2.2. Soft. Tendons, ligaments, or cartilage forms the soft parts of musculoskeletal tissue interfaces. From these tissues, cartilage has the lowest elastic modulus of ∼0.5−1 MPa,[56] withstanding mainly compressive and shear stresses.[125]

Synthetic tendons and ligaments are mainly fabricated from fibrous polymers, made from synthetic (*e.g.*, PLGA) or natural materials (*e.g.*, collagen).[21] Synthetic ligaments have been more widely used than synthetic tendons due to their applications in, for example, ACL and patellar ligament reconstructions. Nonetheless, there has been a substantial decline in the application of these ligaments as a result of inflammatory concerns after prolonged usage.[126]

Generally, biomaterials for cartilage are polymers, such as ultrahigh molecular weight polyethylene (UHMWPE), which can be used for total joint replacements,[127] or other synthetic polymers such as biodegradable polycaprolactone fumarate (PCLF)[128] for scaffolds in tissue regeneration applications.[129] Alternative options are natural polymers made from chitosan,[130] alginate,[131] chondroitin sulfate,[132] hyaluronic acid,[133] fibrin,[134] collagen,[135] gelatin,[136] and decellularized extracellular matrix.[137] In general, the advantage of natural polymers over synthetic polymers is that they are usually biodegradable and biocompatible, whereas synthetic polymers are easily reproducible.[89] However, such natural hydrogel polymers are often softer than synthetic materials, and their composition has a higher batch-to-batch variability, making them less controllable. Besides, the prevalence of non-standardized sterilization procedures across the field risks affecting the properties of natural materials or even containing possible pathogens.[154,163]

Natural polymers are predominantly researched for their favorable biological activities. Furthermore, despite similar water contents and comparable extracellular matrix properties to native cartilage tissues,[22] these natural materials have weak mechanical strength and uncontrollable swelling in aqueous environments which can present problems for osteochondral interface engineering.[22] They are often used as hydrogels. They can be injected at room temperature and form excellent systems for cell-culturing.[138] This makes them useful as a cell delivery system through needle-based minimally invasive surgery. Hydrogels are convenient for repairing small- to medium-sized injuries and mild forms of osteoarthritis.[138]

As mentioned above, the mechanical properties of natural biomaterials are typically lower and less controllable than synthetic biomaterials. This is a major drawback when looking for an implant that can provide a certain mechanical support level within the defect while the tissue regeneration is taking place. Due to a lack of mechanical support, natural biomaterials are often combined with each other to form composite materials or with synthetic biomaterials. For instance, recently, a scaffold based on hyaluronic acid was combined with injectable calcium phosphates (ICPs) to provide the mechanical support that mimics subchondral bone.[133] A cross-linkable oligo(poly(ethylene glycol) fumarate) (OPF)

https://doi.org/10.1021/acsbiomaterials.1c00620
ACS Biomater. Sci. Eng. 2023, 9, 3810−3831

Table 3. Synthetic Bone−Ligament Scaffolds Have Been Manufactured Using Various Techniques and Biomaterials[a]

Study	Material bone	Material ligament	Scaffold type	Processing method	Mechanical properties (tensile)	Biological aspect
190	Brushite cement	Fibrin cement	Bilayered	Casting and anchoring	EM: 5.5 MPA UTS: 42 kPa	*In vivo* study showed that the treatment with ascorbic acid and proline and adding transforming growth factor-β can lead to increase in collagen content which is necessary for ACL reconstruction.
202	PEGDA-hydrogel with HA	PEGDA-hydrogel with HA and RGD	Bilayered	Freeze-drying	EM and YS: In Pascal range	Addition of HA and incorporation of RGD influenced cell attachment and mechanical properties of the interface scaffold.
191	Random porosity- Silk fibroin	Aligned porosity-Silk fibroin	Bilayered	Salt leaching and freeze-drying	EM: 690−1320 kPa	Bilayered scaffolds supported cell attachment. The pore alignment in each region influenced the cytoskeleton organization and the gene expression of tendon/ligament, enthesis, and cartilage markers.
206	PLGA with bioactive glass	Polyglactin-mesh/PLGA	Multilayered (3 layers)	Knitting and sintering	Only compressive tests, no tensile tests. EM (compressive): 110 MPa	The *in vitro* results of the triphasic scaffold exhibited the support of the growth, migration, and phenotypic matrix production of osteoblasts and fibroblasts. Also, the interface scaffold exhibited distinct zonal distributions of cells and phase-specific ECM deposition over time.
194	PLGA with bioactive glass	Polyglactin-mesh/PLGA	Multilayered (3 layers)	Knitting and sintering	Only compressive tests, no tensile tests. EM (compressive): Week 0: 100 MPa Week 8: 85−100 MPa YS (compressive): Week 0: 10 MPa Week 8: 4−4.5 MPa	The *in vivo* results exhibited the formation of distinct yet cellular and matrix regions with various heterogeneity and mineral content.
195	PLGA with bioactive glass	*Transition zone:* PLGA with dichloromethane (DCM) *Ligament:* Polyglactin-mesh	Multilayered (3 layers)	Sintering		The stratified scaffolds were tricultured by osteoblasts, fibroblasts, chondrocytes. The results showed the formation of structurally contiguous and compositionally distinct regions of bone, fibrocartilage and cartilage.
213	PCL	Aligned PLGA-nanofibers	Multilayered (3 layers)	AM and electrospinning	PCL/mixed/PLGA EM: 44/51/89 MPa UTS: 1.6/2.6/5.2 MPa Ultimate strain: 5%/7%/22% elongation	Biological investigation of the scaffolds fabricated by the integration of AM and electrospinning showed a promising approach for regeneration of tissue interfaces.
203	Silk fibroin-Chondroitin Sulfate-HAc with HA	Silk fibroin	Multilayered (3 layers)	Knitting and freeze-drying	Pull-out force: 43 N	The scaffold designs showed an enhanced cell proliferation as well as differentiation when respectively seeded with BMSC, chondrocytes and osteoblasts.
208	Alginate-fibrinogen hydrogel with MSC	Alginate-fibrinogen hydrogel with MSC	Multilayered (3 layers)	Cell-culturing		The *in vivo* implantation results of primed ligament-cartilage-calcified cartilage constructs represented a promising approach for the regeneration of tissue interfaces.
204	PCL with HA	PUR	Gradient	Co-electrospinning	EM: 0.23−2.4 MPa UTS: 0.4−0.62 MPa	Cell studies using an MC3T3-E1 osteoprogenitor verified the biocompatibility of the graded meshes.
205	PCL with HA	PUR	Gradient	Co-electrospinning		The biological studies showed that tuning the mineral content can guide the formation of phenotypic gradient which may promote the regeneration of bone−ligament interface.
60	PCL with cartilage ECM	PCL with ligament ECM	Gradient	Electrospinning and freeze-drying		The microfiber scaffold functionalized with tissue specific (*e.g.*, ligament) ECM guided the differentiation of MSCs toward the bone−ligament phenotypes.
198	PCL-nanofibers with CaP	PCL-nanofibers	Gradient	Electrospinning (2-spinnerets)		Gradient in the content of CaP in nanofiber scaffolds induced a graded response in the adhesion and proliferation of osteogenic cells.
212	Random PLGA-nanofibers	Aligned PCL-nanofibers	Gradient	Electrospinning (multiple spinnerets)	Random EM: 24−28 MPa UTS: 24−25 MPa Aligned	Different fiber orientations in multiple regions resulted in region-dependent cell responses.

https://doi.org/10.1021/acsbiomaterials.1c00620
ACS Biomater. Sci. Eng. 2023, 9, 3810−3831

Table 3. continued

Study	Material bone	Material ligament	Scaffold type	Processing method	Mechanical properties (tensile)	Biological aspect
					EM: 6.8−9.9 MPa UTS: 41−50 MPa	
192	Modified tendon ECM into random organization	Modified tendon ECM into aligned organization	Gradient	Decellularization		The biomimetic tendon ECM (or Random-Aligned-Random) composite scaffold showed enhanced interface properties between bone and fibrocartilage formation in the rabbit ACL reconstruction model *in vivo*.

[a]The acronyms summarized in this table are EM = elastic modulus, UTS = ultimate tensile strength, YS = yield strength, PEGDA = poly(ethylene glycol)diacrylate, HA = hydroxyapatite, RGD = cell adhesion peptide (Arg-Gly-Asp), PLGA = poly(lactide-co-glycolide) acid, DCM = dichloromethane, PCL = polycaprolactone, ECM = extracellular matrix, HAc = hyaluronic acid, MSC = mesenchymal stem cells, PUR = polyurethane, RGD = red adhesion peptide, BMSC = bone marrow mesenchymal stem cells.

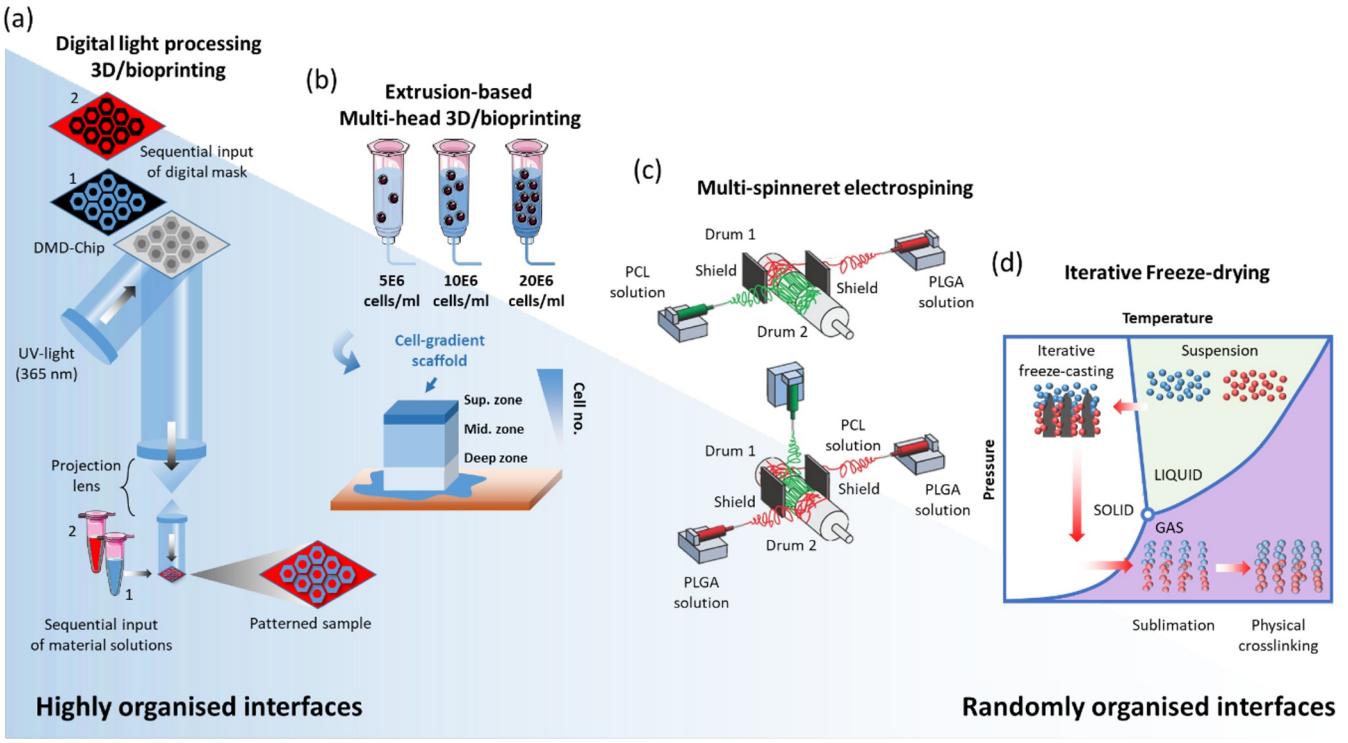

Figure 3. Schematics of different fabrication methods that can be used for bone-to-soft interfaces, from highly organized interfaces (left) to randomly organized interfaces (right). (a) Digital light processing-based 3D/bioprinting showing that sequential input of different digital masks can be used to generate patterns with interfaces of different materials. Panel a is reproduced with permission from ref 186. Copyright 2021 National Academy of Sciences. (b) Extrusion-based 3D/bioprinting showing that the combination of multiheads containing different bioinks can be used to generate scaffolds with gradients (in this example, cell gradients mimicking articular cartilage cell density. Panel b is reproduced with permission from ref 187. Copyright 2021 MDPI. (c) Electrospinning setup with two spinnerets creating a transitory region. Reproduced with permission from ref 212. Copyright 2021 John Wiley and Sons. (d) Iterative freeze-casting (or ice-templating) can be combined with freeze-drying to achieve bilayered structures with a defined interface.

has been used as a scaffold combined with gelatin microparticles to deliver chondrogenic or osteogenic factors.[136] Also composites of natural materials, such as fibrous collagen with hyaluronic acid, have demonstrated very special and favorable properties and show promise for future design of scaffolds.[139]

3.3. Fabrication Techniques of BSTIs' Scaffolds. Here, we focus on the design and mechanical properties of state-of-the-art interface scaffolds as a consequence of their specific requirements and target tissues (*i.e.*, bone−cartilage (Table 1), bone−tendon (Table 2), and bone−ligament (Table 3) interfaces). The scaffold composition's effects on cell regeneration and tissue integration have been reviewed elsewhere.[21,41,53,140]

Various studies and reviews have focused on engineering single musculoskeletal tissues such as bone, tendon, ligament, cartilage, or muscle, using confined monolithic scaffolds.[141−144] They have attempted to find an optimal combination of chemical and mechanical factors to regenerate the underlying tissues. Despite promising results, it remains challenging to regenerate these single tissues.[145] To engineer BSTIs, monolithic scaffolds will not suffice. Fabrication methods, materials, and the mechanical properties of the fabricated BSTIs' monolithic scaffolds are given in Tables 1 and 2. Interface scaffolds will require at least two separate parts containing the appropriate cues for each type of tissue.

https://doi.org/10.1021/acsbiomaterials.1c00620
ACS Biomater. Sci. Eng. 2023, 9, 3810−3831

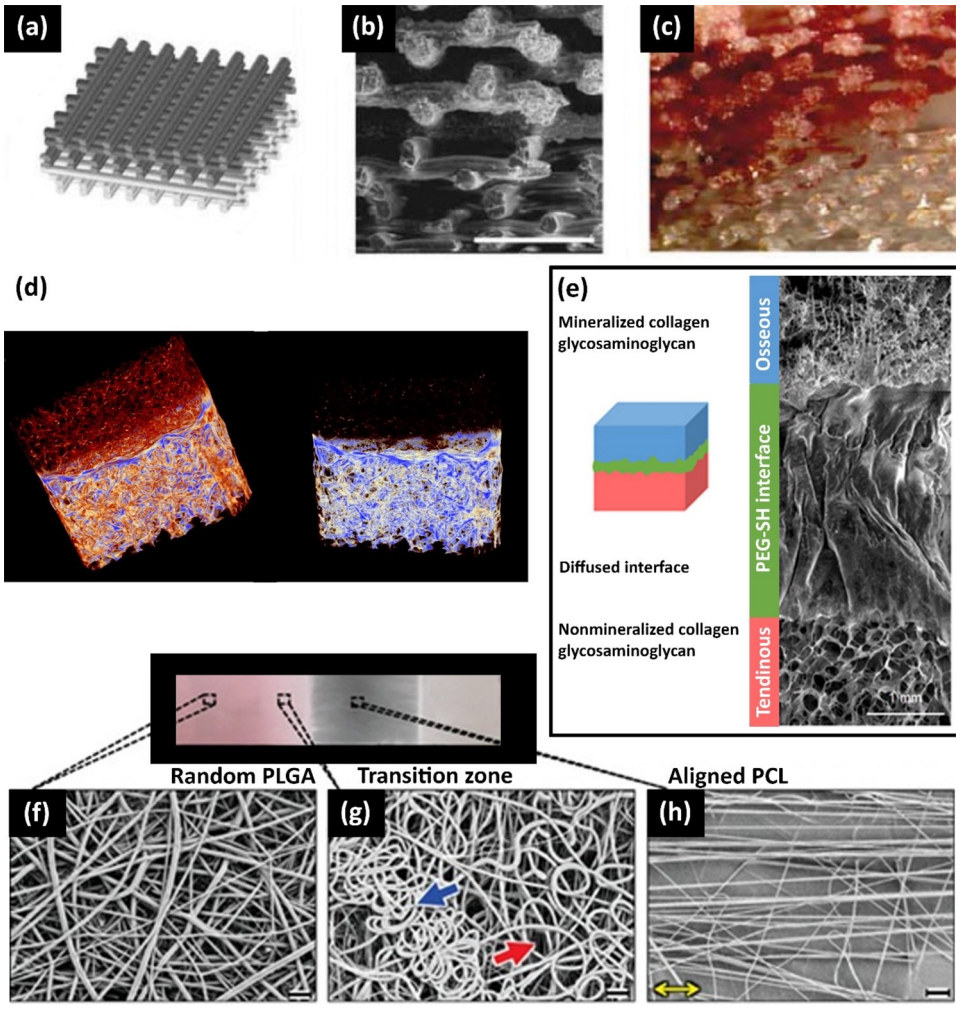

Figure 4. (a–c) Extrusion-based 3D printing of osteochondral interface scaffold: (a) CAD design, (b) interface of PLA and a PLA/bioglass bilayer, (c) scaffold microstructure stained with alizarin. Panels a–c are reproduced with permission from ref 118. Copyright 2021 Elsevier. (d) Freeze-dried bilayered silk and silk-nano CaP scaffolds for the osteochondral interface. Panel d is reproduced with permission from ref 15. Copyright 2021 Elsevier. (e) Freeze-dried triphasic structural-continuous scaffolds made of the mineralized, diffused region and nonmineralized collagen glycosaminoglycan for the bone–tendon interface. Panel e is reproduced with permission from ref 214. Copyright 2021 Science Advances. Electrospun enthesis scaffolds made of PLGA-PCL with a graded design from (f) the random PLGA region, (g) the transition of PLGA to the PCL region, to (h) the aligned PCL region. Panels f–h are reproduced with permission from ref 212. Copyright 2021 John Wiley and Sons.

Additionally, it is desirable to dedicate parts of the scaffold to the different transition zone regions, thereby involving at least multilayered or gradient scaffolds (Figure 2b). Multilayered scaffolds allow for applying various materials, architectural structures, and cell types per region of the interface. The discrete layers are joined together by gluing, suturing, or knitting,[146] hindering a smooth transition between layers.[6,21,146] Therefore, the layers have to be joined together with significant care to prevent problems with the mechanical integration and interconnectivity of different regions.[6] Gradient scaffolds can prevent these problems, introducing gradual transitions between the other regions, similar to native interfaces. However, due to the geometrical complexity of FGMs, the manufacturing of these structures using conventional fabrication techniques can become quite challenging. Therefore, it requires more specialized processing methods to fabricate FGMs. Frequently used techniques are vapor deposition techniques, metal foaming techniques, powder metallurgy, centrifugal methods, space-holder methods, and AM techniques.[99,104] However, due to insufficient control over these techniques, most of them can only fabricate randomly organized structures (Figure 3). This significantly limits the possible compositional, microstructural, and porous arrangement of the materials. The only techniques that can be distinguished are AM techniques due to high control over material placement accuracy and precision.[104] In this case, the methods are named functionally graded additive manufacturing (FGAM), relying on a layer-by-layer fabrication process to strategically control material placement[147] as schematically illustrated in Figure 3a and b.

It has been demonstrated that cell organization is strongly influenced by the topography and mechanical properties of the environment.[148−152] Cells have been shown to align themselves in a dominant direction, for which it has been hypothesized that this is a mechanism to avoid stresses.[153] The net disassembly of stress fibers parallel to an imposed strain results in cytoskeletal alignment perpendicular to that strain.[154−156] In turn, this environment-controlled orientation leads to the production of an oriented matrix.[157,158] It has been shown that the scaffold architecture can determine the

https://doi.org/10.1021/acsbiomaterials.1c00620
ACS Biomater. Sci. Eng. 2023, 9, 3810−3831

deposited collagen network's organization by fibroblasts, with a fiber orientation parallel to the major cell axis.[159,160] In addition, cellular and neo-matrix alignment within decellularized cartilage explants seems to be affected by the underlying collagen architecture of the decellularized tissue.[161] The newly deposited organized tissue has been demonstrated to play a role in different events of tissue development. For instance, the *de novo* deposited aligned matrix of a scaffold made of collagen type I influenced the mineral to align in the fiber orientation direction[162] after inducing endochondral healing in a rat femoral defect.

Scaffolds with aligned architecture have also been tested for other tissues with an anisotropic nature, such as tendons or ligaments.[163] An engineered construct that matches the hierarchical structure of the native ACL has sufficient mechanical properties and encourages the production of ligamentous tissue deposition, which is hypothesized to improve the clinical treatment of ACL injuries.[164] In addition, scaffolds containing cylindrical pores result in greater compressive moduli in comparison with constructs with more isotropic spherical pores, avoiding cell-mediated contraction and enabling complex maintenance for three-dimensional structures[165] with stabilized mechanical properties.[166,167] Anisotropic structures may also provide further benefits, such as encouraging cell infiltration[168] or facilitating the transport of nutrients and the exchange of metabolites in the porous scaffolds. The latest may be due to the oriented, congruently aligned, and interlinked fiber structures.[169] Recent studies have also demonstrated the importance of scaffold pore anisotropy and pore size on the quality and organization of scaffold fabrication and hence their enhanced long-term performance.[168,169]

3.3.1. Osteochondral Scaffolds. The average length of the osteochondral interface is from 50 μm to 1 mm depending on species and age,[40,41] with a highly structured and geometrically complex tissue on a relatively small scale. Thus, the characterization and recapitulation of the interface represent a significant challenge to the current viable technologies to study and fabricate multimaterial structures.

Osteochondral tissue engineering has relied mostly on bilayered[170−172] and multilayered[173,174] scaffolds instead of graded scaffolds as given under the fabrication methods in Table 1. Most of these osteochondral scaffolds are made of polymeric materials and hydrogels, where necessary reinforced with fibers or microparticles. The most prominent particle enhancing the mechanical properties of the bony layer has been HA. Particles made from HA are well-known for its chemical resemblance to the inorganic constituent of bone tissues. The favorable properties of HA are high bioactivity and osteoconductivity, nontoxic and noninflammatory properties, and angiogenic properties.[175] Therefore, HA forms an attractive biomaterial due to its high biocompatibility and superior ability to integrate with bone tissues.[176]

Osteochondral scaffolds have been fabricated through a number of techniques such as sintering,[120] gelling,[177] salt-leaching,[15,178] AM (*e.g.*, fused deposition modeling (FDM) or bioprinting) (Figure 3b),[23,24,179] (iterative) freeze-drying (lyophilization) (Figure 3d),[137,180,181] and casting and diffusion.[182] The selection of these techniques depends highly on the biomaterials of choice and desired architecture. For instance, techniques such as freeze-drying allow for the fabrication of tailorable interconnected micro- and nanopores, which has been shown to modulate cell infiltration in endochondral healing of bone defects.[162]

In addition, freeze-drying has been reported as a successful technique to create osteochondral bilayers with a stable interface through an iterative freezing technique.[137] The melting and refreezing of the different phases allow for creating an interface in which fiber entanglement from each layer creates a geometrically interlocking structure. On the other hand, techniques such as salt-leaching, gelling, or sintering depend on casting the material into a prefabricated mold and its posterior removal from the mold, which limit the complexity of structures that can be fabricated. Therefore, over recent years, AM techniques have been gaining popularity due to their high fidelity and resolution, enabling the fabrication of complex geometrical scaffolds with deeply interconnected porosity. This allows for the construction of osteochondral interfaces with locally changing properties in a single 3D-construct (Figure 4a−d).

The osteochondral scaffolds fabricated with AM have primarily been made from synthetic polymers (*i.e.*, PCL,[24,115] (polyglycolic acid)PGA/PLA,[115] and PLA[118]) and different hydrogel mixtures.[22,23,183] One of the reasons for the popularity of PLA is that it allows for quick fabrication of scaffolds through AM techniques without high inflammatory responses in the human body.[118] The disadvantages are reduced bioactivity levels, resulting in a weak bonding with bone.[184]

Osteochondral scaffolds need to have mechanical stability and controllable degradation rates in order to maintain their initial shape and mechanical properties in load-bearing environments, such as the knee joint. Mechanical strength provides the opportunity and necessary time frame for native tissues to regenerate. Overall, the osteochondral scaffolds have a stiffness ranging from 5 kPa to 140 MPa (Table 1), depending on their biomaterials and fabrication methods. From a mechanical perspective, the scaffolds designed by Shalumon et al. (2016),[120] Ding et al. (2013),[115] and Barbeck et al. (2017)[118] have the most promising mechanical properties, offering the required structural support for tissue regeneration. The PLGA-scaffolds reinforced with HA-particles and manufactured by Shalumon et al. (2016) possess by far the highest mechanical strength of all the osteochondral scaffolds summarized in Table 1. These scaffolds were built by combining casting and sintering, resulting in a stiffness of 142 MPa for the bony layer and 62 MPa for the cartilage layer.[120] Additionally, PLGA can be used to encapsulate chemical substances and proteins in biodegradable microspheres. These microspheres are then sintered into a scaffold and function as a controlled delivery system to release proteins, peptides, growth factors, small molecules, and other chemotherapeutic agents.[185]

Ding et al. (2013) tailored the stiffness of the PCL-scaffolds and PGA-scaffolds, with HA and PLA, respectively, to obtain a matrix stiffness that mimicked part of the mechanical properties of native bone and cartilage. The stiffness was 58 MPa for the bony layer and 5 MPa for the cartilage layer.[115] Other relatively stiff scaffolds fabricated with AM techniques are the PLA-scaffolds by Barbeck et al. (2017). The stiffness of these scaffolds was 44 MPa for the bony layer and 28 for the cartilage layer.[118]

Natural polymers such as hydrogels (*e.g.*, alginate, agarose, poly(ethylene glycol) methacrylate (PEGMA), and gelatin methacrylate (GelMA)[183]) have also been successfully used in

https://doi.org/10.1021/acsbiomaterials.1c00620
ACS Biomater. Sci. Eng. 2023, 9, 3810−3831

3D printing of cartilage scaffolds. Generally, 3D (bio)-printing[186,187] takes advantage of a layer-by-layer technique to create tissue-like architectures that can be cross-linked to increase the structural stability. However, as previously mentioned, hydrogel scaffolds lack the mechanical properties for demanding load-bearing environments. Several studies have combined stiff polymeric scaffolds with casted or 3D-printed hydrogels to provide a mechanically stable structure as well as a biomimetic cell environment.[188,189] Recently, a high-strength thermoresponsive supramolecular copolymer hydrogel has been synthesized and 3D printed for osteochondral tissue applications demonstrating superior mechanical properties to traditional hydrogel scaffolds with high tensile strength (up to 0.41 MPa), compressive strength (up to 8.4 MPa), and stretchability (up to 860%).[22]

3.3.2. Enthesis Scaffolds. Enthesis scaffolds have relied mostly on multilayered and graded scaffold designs; see Tables 2 and 3 for further information about the materials, fabrication methods, and mechanical properties of these scaffolds. The grand majority of scaffolds are made from fiber-based materials, mimicking the fibrous collagen networks in tendons and ligaments (Figure 4e).[20,190−192] Since collagen is the most plentiful protein in human connective tissues,[181] it has been studied most often. Furthermore, replicating the hierarchical organization of collagenous tissues through self-assembling fiber-based biomaterials[193] could be of great use for enthesis tissue engineering. However, translating these natural features into a complex multilayered scaffold requires a biomimetic approach and remains challenging.

The most commonly used biomaterials for the fabrication of fibers are the synthetic polymers PLGA[194−196] and PCL.[32,197,198] In contrast to osteochondral interface engineering, natural biomaterials and hydrogels are less frequently used for enthesis tissue engineering. Combining synthetic fibers with ceramic particles makes it possible to mineralize fibers to improve their mechanical properties. Frequently used ceramic particles are calcium phosphates (CaP),[13,196,198] HA,[31,199−205] and bioactive glasses.[194,195,206,207] It is also possible to combine natural or synthetic polymers with tissue-specific extracellular matrices[208] for enhancing tissue regeneration. The ECM consists of structural and regulatory biomolecules that promote the differentiation of multiple cell phenotypes and the biological function of native tissues while being located in mechanically functional scaffolds.[60]

The degree of mineralization (*e.g.*, mineral coating) of individual (nano)fibers as well as their morphology (*e.g.*, cross section) and distributions (*e.g.*, random, ordered) highly influence the macroscopic mechanical properties (*i.e.*, elastic moduli, strength, and toughness) of the enthesis scaffolds. By gradually increasing the mineralization level of polymer fibers, it is possible to create gradients in the mechanical properties. Although the mineralization of fibers increases the stiffness, the realized peak stiffness remains significantly below that of bone tissue. The highest stiffness values were reported by Kolluru et al. (2013) and Lipner et al. (2014) at ∼2.5 GPa[199] and ∼3.1 GPa,[200] respectively, whereas the stiffness of bone tissue is ∼17−21 GPa.[55,56] This difference in stiffness is partly because the minerals cannot penetrate polymer fibers and only attach to the surface. Therefore, it is vital that the mineral coating is dense and well-bonded to the fiber; otherwise, little amount of stress can be transferred, and the fibers remain compliant. Besides, the coating has to be continuous for the fibers to carry the loads.[200] Mineral coating of PLGA nanofibers improves the mechanical properties of PLGA. It has been demonstrated that the failure strength of mineralized PLGA nanofibers is similar to the bone tissue. Increased fiber−fiber bonding through mineral cross-bridges is one method of mineralization to influence the network properties and thus to improve the scaffold's mechanical properties.[199]

A different approach to create biomimetic gradients is to strategically manipulate the fiber orientation.[197,209−213] This strategy relies on the region-wise architectural transition from aligned-to-random fiber orientations, representing the tendon and bone layers, respectively (Figure 4f−h). Additionally, it is possible to create a transition zone by varying the structure and composition of fibers,[197,212,213] resulting in a graded structure that can offer interface sustainability while transferring stress between mechanically dissimilar materials. For this strategy, electrospinning (Figure 3c) was a very suitable fabrication method because relatively simple adjustments to the setup result in the desired fiber orientations.[197,210,212] From an aligned-to-random fiber orientation, the stiffness changes approximately with a factor of 3 from ∼50 MPa to ∼150 MPa.[210] The overall stiffness of these scaffolds depends highly on their precise material composition and structure, with a peak stiffness of 350 MPa in a PLGA-based scaffold.[209]

A recent study by Sun Han Chang et al. (2020) showed that the addition of a compliant interface (hydrogel) between different scaffolds (*i.e.*, mineralized and nonmineralized collagen scaffold) provides a bioinspired approach that improves the mechanical performance of the enthesis by effectively dissipating local strains.[214] The compliant zone reduced the prevalence of failure between mechanically mismatched tissue compartments, validating previous observations on the structure−function properties of native entheses.[5,80,81]

The most frequently used fabrication methods for enthesis scaffolds are electrospinning techniques (Figure 3c). Electrospinning is a method for fiber production that uses electric forces to draw positively charged threads of polymer solutions or melts through a thin needle. A target attached to the surface or a negative voltage attracts the solution, determining the fiber orientation. Stationary targets produce random fiber orientations, whereas spinning targets produce aligned fiber orientations.[197,215] These techniques can make nanoscale fibers from synthetic polymers. The resulting fibers have been shown to have high surface-to-volume ratio, tunable porosity, and the abilities to adapt to a wide variety of shapes and to manipulate the fiber composition to create desired properties and functions.[215] However, these techniques have limitations as they require high voltages, challenging the ability to incorporate living cells into the scaffolds.[193] Also, the necessary solvents and high processing temperatures can denature the structure of natural polymers.[216,217] This makes it problematic to include polymers from natural sources, such as collagen and chitosan, into scaffolds. Wet-spinning is a form of electrospinning that converts molecules into nanofibers without the need for toxic solvents, high voltages, or temperatures. This allows for better cell-culturing conditions and the possibility to incorporate natural polymers into the scaffolds.[31] For this reason, an originally textile technique is being examined for biomedical applications.[31,218]

Considering the high geometrical complexity of enthesis scaffolds, it is remarkable that AM is very rarely used to fabricate them. Part of this is because mimicking the hierarchical fiber organization of enthesis tissues requires a

https://doi.org/10.1021/acsbiomaterials.1c00620
ACS Biomater. Sci. Eng. 2023, 9, 3810−3831

fiber diameter in the range of ∼300−1000 nm.[199] While electrospinning techniques can fabricate fibers between 100 nm and 1 μm,[197] the highest possible resolution for AM techniques is in the upper micron range.[219] This is insufficient to recreate the hierarchical fiber organization of native tissues. Additionally, the fiber diameter influences the cell orientation and morphology by a phenomenon called "contact guidance". This phenomenon suggests that regional differences in fiber orientation lead to regional differences in the shape, orientation, and phenotype of adherent cells.[212] This makes it crucial to manufacture scaffolds with appropriate fiber diameter and organization.

An alternative option for enthesis tissue engineering is to manufacture multistructured constructs through a combination of fabrication methods and biomaterials. Such combinations can increase the range of attainable mechanical properties. For example, Laurent et al. (2018)[143] worked on a bone−ligament interface tissue-engineered construct that regenerates bone and ligament tissues by applying different mechanical stimuli to the scaffold's different regions during a midterm culture. The discussed tissue regeneration method has been realized by a 3D-printed screw-shaped bone insertion and intermediate conical-shaped bone scaffold that allowed for compressive loading at the bone level (Figure 2d). In contrast, an electrospun fibrous ligament scaffold allowed tensile loading at the ligament level.[143] This shows how strategic design combinations can lead to innovations in the field of tissue interface engineering.

Similar to osteochondral scaffolds, the current challenge for enthesis tissue engineering is to bridge the gap between these widely different tissues over such a small length scale while maintaining the scaffold's structural integrity under load. Additionally, the scaffold has to enable a good integration of the repaired tissue with the surrounding tissues.

4. CONCLUDING REMARKS AND FUTURE PERSPECTIVES

Natural hard−soft interfaces outperform human-made interfaces due to their multifunctional capabilities on a small length scale. The natural interfaces exhibit gradual transition in the degrees of mineralization from one tissue to another at several length scales, making it hard to replicate them. A good perception of the chemical and mechanical principles behind natural hard−soft interfaces can lead to improved bone-to-soft tissue scaffolds, advancing the field of tissue interface engineering.

To manufacture replacements for BSTIs, it is important to choose appropriate fabrication methods and biomaterials for each specific case. While osteochondral scaffolds have been fabricated by a wide range of fabrication techniques and materials, enthesis scaffolds have almost exclusively relied on electrospun PLGA- and PCL-fibers. Recently, AM techniques have become increasingly popular fabrication methods for osteochondral interface engineering. This is due to their high spatiotemporal resolution and its potential ability to print multiple materials at once, allowing for the fabrication of more complex structures. AM uses computer-aided design (CAD) models to print 3D-scaffolds. These models can be analyzed for the mechanical performance and optimization of the material layout. The models can be improved through computer simulations, providing better future studies' outcomes in a shorter time frame.

Essential mechanical properties have been the stiffness and strength of bone-to-soft tissue interfaces. However, it should be noted that the interfacial strength is not the only property determining the long-term performance of these interfaces. As observed in Nature, a compliant zone between materials can provide favorable outcomes. Therefore, to create structures with an appropriate stiffness, their toughness and ductility also have to be considered.

Further research is needed to develop advanced BSTIs, fitting all the requirements. Besides studying the mechanical behavior of various interlocking principles, further study on the other influencing parameters on such a system is required. To fulfill this, it is necessary to combine engineering and biology knowledge and create biomimetic designs of interface scaffolds to regenerate BSTIs successfully. Research on cell−matrix interactions and mechanotransduction should provide more insight in cellular behavior in BSTI scaffolds to stimulate the regeneration of a proper interface that will provide long-term functional tissue.

Besides the regeneration of BSTIs, there is a lack of solutions to connect dissimilar materials. Possible solutions can be drawn from common geometrically patterned interfaces, increasing the strength, toughness, and damage tolerance features of natural interlocking designs. The best performing designs have been triangular and antitrapezoidal patterns. A strong case has also been made for additive fractal patterns and surface roughness, mimicking the structural hierarchy found in Nature. Possible mechanisms for the improved performance of these interfaces are enhanced energy dissipation, increased shear forces at the interface, and more homogeneous stress distribution. A further increment of the shear forces at the interface can be achieved through adhesive coatings. Also, further investigations on applications and fabrications of FGMs for designing BSTIs are required.

AUTHOR INFORMATION

Corresponding Author

Mohammad J. Mirzaali − *Department of Biomechanical Engineering, Faculty of Mechanical, Maritime and Materials Engineering, Delft University of Technology, 2628 CD Delft, The Netherlands*; orcid.org/0000-0002-5349-6922; Phone: +31-15-2783133; Email: m.j.mirzaali@tudelft.nl

Authors

Carlos Pitta Kruize − *Department of Biomechanical Engineering, Faculty of Mechanical, Maritime and Materials Engineering, Delft University of Technology, 2628 CD Delft, The Netherlands*

Sara Panahkhahi − *Department of Biomechanical Engineering, Faculty of Mechanical, Maritime and Materials Engineering, Delft University of Technology, 2628 CD Delft, The Netherlands*

Niko Eka Putra − *Department of Biomechanical Engineering, Faculty of Mechanical, Maritime and Materials Engineering, Delft University of Technology, 2628 CD Delft, The Netherlands*; orcid.org/0000-0003-4620-9785

Pedro Diaz-Payno − *Department of Biomechanical Engineering, Faculty of Mechanical, Maritime and Materials Engineering, Delft University of Technology, 2628 CD Delft, The Netherlands*

Gerjo van Osch − *Department of Biomechanical Engineering, Faculty of Mechanical, Maritime and Materials Engineering,*

https://doi.org/10.1021/acsbiomaterials.1c00620
ACS Biomater. Sci. Eng. 2023, 9, 3810−3831

Delft University of Technology, 2628 CD Delft, The Netherlands

Amir A. Zadpoor − *Department of Biomechanical Engineering, Faculty of Mechanical, Maritime and Materials Engineering, Delft University of Technology, 2628 CD Delft, The Netherlands;* orcid.org/0000-0003-3234-2112

Complete contact information is available at: https://pubs.acs.org/10.1021/acsbiomaterials.1c00620

Notes

The authors declare no competing financial interest.

■ ACKNOWLEDGMENTS

Mohammad J. Mirzaali acknowledges funding from the Dutch Research Agenda through Idea Generator Research programme (NWA-IDG) file number NWA.1228.192.228.

■ REFERENCES

(1) Waite, J. H.; Lichtenegger, H. C.; Stucky, G. D.; Hansma, P. Exploring molecular and mechanical gradients in structural bioscaffolds. *Biochemistry* **2004**, *43* (24), 7653−7662.

(2) Mirzaali, M. J.; Herranz de la Nava, A.; Gunashekar, D.; Nouri-Goushki, M.; Doubrovski, E.; Zadpoor, A. A. Fracture behavior of bioinspired functionally graded soft−hard composites made by multi-material 3D printing: the case of colinear cracks. *Materials* **2019**, *12* (17), 2735.

(3) Rao, R. T.; Browe, D. P.; Lowe, C. J.; Freeman, J. W. An overview of recent patents on musculoskeletal interface tissue engineering. *Connect. Tissue Res.* **2016**, *57* (1), 53−67.

(4) Armitage, O. E.; Oyen, M. L. Indentation across interfaces between stiff and compliant tissues. *Acta Biomater.* **2017**, *56*, 36−43.

(5) Rossetti, L.; Kuntz, L.; Kunold, E.; Schock, J.; Müller, K.; Grabmayr, H.; Stolberg-Stolberg, J.; Pfeiffer, F.; Sieber, S.; Burgkart, R. The microstructure and micromechanics of the tendon−bone insertion. *Nat. Mater.* **2017**, *16* (6), 664.

(6) Armitage, O. E.; Oyen, M. L. Hard-soft tissue interface engineering. In *Engineering Mineralized and Load Bearing Tissues*; Springer: 2015; pp 187−204.

(7) Seidi, A.; Ramalingam, M.; Elloumi-Hannachi, I.; Ostrovidov, S.; Khademhosseini, A. Gradient biomaterials for soft-to-hard interface tissue engineering. *Acta Biomater.* **2011**, *7* (4), 1441−1451.

(8) Boys, A. J.; McCorry, M. C.; Rodeo, S.; Bonassar, L. J.; Estroff, L. A. Next generation tissue engineering of orthopedic soft tissue-to-bone interfaces. *MRS Commun.* **2017**, *7* (3), 289−308.

(9) Galatz, L. M.; Sandell, L. J.; Rothermich, S. Y.; Das, R.; Mastny, A.; Havlioglu, N.; Silva, M. J.; Thomopoulos, S. Characteristics of the rat supraspinatus tendon during tendon-to-bone healing after acute injury. *J. Orthop. Res.* **2006**, *24* (3), 541−550.

(10) Galatz, L. M.; Ball, C. M.; Teefey, S. A.; Middleton, W. D.; Yamaguchi, K. The outcome and repair integrity of completely arthroscopically repaired large and massive rotator cuff tears. *JBJS* **2004**, *86* (2), 219−224.

(11) Chen, J.; Xu, J.; Wang, A.; Zheng, M. Scaffolds for tendon and ligament repair: review of the efficacy of commercial products. *Expert Rev. Med. Devices* **2009**, *6* (1), 61−73.

(12) Bicho, D.; Pina, S.; Reis, R. L.; Oliveira, J. M. Commercial Products for Osteochondral Tissue Repair and Regeneration. In *Osteochondral Tissue Engineering*; Springer: 2018; pp 415−428.

(13) Li, X.; Xie, J.; Lipner, J.; Yuan, X.; Thomopoulos, S.; Xia, Y. Nanofiber scaffolds with gradations in mineral content for mimicking the tendon-to-bone insertion site. *Nano Lett.* **2009**, *9* (7), 2763−2768.

(14) Levingstone, T. J.; Thompson, E.; Matsiko, A.; Schepens, A.; Gleeson, J. P.; O'Brien, F. J. Multi-layered collagen-based scaffolds for osteochondral defect repair in rabbits. *Acta Biomater.* **2016**, *32*, 149−160.

(15) Yan, L.-P.; Silva-Correia, J.; Oliveira, M. B.; Vilela, C.; Pereira, H.; Sousa, R. A.; Mano, J. F.; Oliveira, A. L.; Oliveira, J. M.; Reis, R. L. Bilayered silk/silk-nanoCaP scaffolds for osteochondral tissue engineering: in vitro and in vivo assessment of biological performance. *Acta Biomater.* **2015**, *12*, 227−241.

(16) Scaffaro, R.; Lopresti, F.; Maio, A.; Sutera, F.; Botta, L. Development of polymeric functionally graded scaffolds: A brief review. *J. Appl. Biomater. Funct. Mater.* **2017**, *15* (2), 107−121.

(17) Xue, D.; Zheng, Q.; Zong, C.; Li, Q.; Li, H.; Qian, S.; Zhang, B.; Yu, L.; Pan, Z. Osteochondral repair using porous poly (lactide-co-glycolide)/nano-hydroxyapatite hybrid scaffolds with undifferentiated mesenchymal stem cells in a rat model. *J. Biomed. Mater. Res., Part A* **2010**, *94* (1), 259−270.

(18) Reyes, R.; Delgado, A.; Sanchez, E.; Fernandez, A.; Hernandez, A.; Evora, C. Repair of an osteochondral defect by sustained delivery of BMP-2 or TGFβ1 from a bilayered alginate−PLGA scaffold. *J. Tissue Eng. Regener. Med.* **2014**, *8* (7), 521−533.

(19) Jiang, J.; Tang, A.; Ateshian, G. A.; Guo, X. E.; Hung, C. T.; Lu, H. H. Bioactive stratified polymer ceramic-hydrogel scaffold for integrative osteochondral repair. *Ann. Biomed. Eng.* **2010**, *38* (6), 2183−2196.

(20) Calejo, I.; Costa-Almeida, R.; Reis, R. L.; Gomes, M. E. A Physiology-Inspired Multifactorial Toolbox in Soft-to-Hard Musculoskeletal Interface Tissue Engineering. *Trends Biotechnol.* **2020**, *38*, 83.

(21) Cross, L. M.; Thakur, A.; Jalili, N. A.; Detamore, M.; Gaharwar, A. K. Nanoengineered biomaterials for repair and regeneration of orthopedic tissue interfaces. *Acta Biomater.* **2016**, *42*, 2−17.

(22) Gao, F.; Xu, Z.; Liang, Q.; Liu, B.; Li, H.; Wu, Y.; Zhang, Y.; Lin, Z.; Wu, M.; Ruan, C. Direct 3D printing of high strength biohybrid gradient hydrogel scaffolds for efficient repair of osteochondral defect. *Adv. Funct. Mater.* **2018**, *28* (13), 1706644.

(23) Hu, X.; Man, Y.; Li, W.; Li, L.; Xu, J.; Parungao, R.; Wang, Y.; Zheng, S.; Nie, Y.; Liu, T. 3D Bio-Printing of CS/Gel/HA/Gr Hybrid Osteochondral Scaffolds. *Polymers* **2019**, *11* (10), 1601.

(24) Li, L.; Li, J.; Guo, J.; Zhang, H.; Zhang, X.; Yin, C.; Wang, L.; Zhu, Y.; Yao, Q. 3D molecularly functionalized cell-free biomimetic scaffolds for osteochondral regeneration. *Adv. Funct. Mater.* **2019**, *29* (6), 1807356.

(25) Mirzaali, M. J.; Cruz Saldívar, M.; Herranz de la Nava, A.; Gunashekar, D.; Nouri-Goushki, M.; Doubrovski, E. L.; Zadpoor, A. A. Multi-material 3D printing of functionally graded hierarchical soft−hard composites. *Adv. Eng. Mater.* **2020**, *22* (7), 1901142.

(26) Putra, N.; Mirzaali, M.; Apachitei, I.; Zhou, J.; Zadpoor, A. Multi-material additive manufacturing technologies for Ti-, Mg-, and Fe-based biomaterials for bone substitution. *Acta Biomater.* **2020**, *109*, 1−20.

(27) Mirzaali, M.; de la Nava, A. H.; Gunashekar, D.; Nouri-Goushki, M.; Veeger, R.; Grossman, Q.; Angeloni, L.; Ghatkesar, M.; Fratila-Apachitei, L.; Ruffoni, D. Mechanics of bioinspired functionally graded soft-hard composites made by multi-material 3D printing. *Composite Structures* **2020**, *237*, 111867.

(28) Mirzaali, M. J.; Edens, M. E.; de la Nava, A. H.; Janbaz, S.; Vena, P.; Doubrovski, E. L.; Zadpoor, A. A. Length-scale dependency of biomimetic hard-soft composites. *Sci. Rep.* **2018**, *8* (1), 12052.

(29) Gu, G. X.; Su, I.; Sharma, S.; Voros, J. L.; Qin, Z.; Buehler, M. J. Three-dimensional-printing of bio-inspired composites. *J. Biomech. Eng.* **2016**, *138* (2), DOI: 10.1115/1.4032423.

(30) Nie, X.; Chuah, Y. J.; He, P.; Wang, D.-A. Engineering a multiphasic, integrated graft with a biologically developed cartilage−bone interface for osteochondral defect repair. *J. Mater. Chem. B* **2019**, *7* (42), 6515−6525.

(31) Calejo, I.; Costa-Almeida, R.; Reis, R. L.; Gomes, M. E. A Textile Platform Using Continuous Aligned and Textured Composite Microfibers to Engineer Tendon-to-Bone Interface Gradient Scaffolds. *Adv. Healthcare Mater.* **2019**, *8* (15), 1900200.

(32) Tarafder, S.; Brito, J. A.; Minhas, S.; Effiong, L.; Thomopoulos, S.; Lee, C. H. In situ tissue engineering of the tendon-to-bone interface by endogenous stem/progenitor cells. *Biofabrication* **2020**, *12* (1), 015008.

(33) Liu, Z.; Meyers, M. A.; Zhang, Z.; Ritchie, R. O. Functional gradients and heterogeneities in biological materials: Design principles, functions, and bioinspired applications. *Prog. Mater. Sci.* **2017**, *88*, 467−498.
(34) Link, J. M.; Salinas, E. Y.; Hu, J. C.; Athanasiou, K. A. The tribology of cartilage: Mechanisms, experimental techniques, and relevance to translational tissue engineering. *Clin Biomech (Bristol, Avon)* **2020**, *79*, 104880.
(35) Beck, E. C.; Barragan, M.; Tadros, M. H.; Gehrke, S. H.; Detamore, M. S. Approaching the compressive modulus of articular cartilage with a decellularized cartilage-based hydrogel. *Acta Biomater.* **2016**, *38*, 94−105.
(36) Gardner-Morse, M. G.; Tacy, N. J.; Beynnon, B. D.; Roemhildt, M. L. In situ microindentation for determining local subchondral bone compressive modulus. *J. Biomech. Eng.* **2010**, *132* (9), 094502.
(37) Lyons, T. J.; Stoddart, R. W.; McClure, S. F.; McClure, J. The tidemark of the chondro-osseous junction of the normal human knee joint. *J. Mol. Histol.* **2005**, *36* (3), 207−215.
(38) Bian, W.; Lian, Q.; Li, D.; Wang, J.; Zhang, W.; Jin, Z.; Qiu, Y. Morphological characteristics of cartilage-bone transitional structures in the human knee joint and CAD design of an osteochondral scaffold. *BioMed. Eng. OnLine* **2016**, *15* (1), 82.
(39) Imhof, H.; Breitenseher, M.; Kainberger, F.; Rand, T.; Trattnig, S. Importance of subchondral bone to articular cartilage in health and disease. *Top Magn Reson Imaging* **1999**, *10* (3), 180−92.
(40) Yang, P. J.; Temenoff, J. S. Engineering orthopedic tissue interfaces. *Tissue Eng., Part B* **2009**, *15* (2), 127−141.
(41) Di Luca, A.; Van Blitterswijk, C.; Moroni, L. The osteochondral interface as a gradient tissue: From development to the fabrication of gradient scaffolds for regenerative medicine. *Birth Defects Res., Part C* **2015**, *105* (1), 34−52.
(42) Chen, Q.; Thouas, G. Metallic implant biomaterials. *Mater. Sci. Eng., R* **2015**, *87*, 1−57.
(43) Zhang, Y.; Wang, F.; Tan, H.; Chen, G.; Guo, L.; Yang, L. Analysis of the mineral composition of the human calcified cartilage zone. *Int. J. Med. Sci.* **2012**, *9* (5), 353−360.
(44) Dijk, C. N.; Mueller-Gerbl, M. The basic science of the subchondral bone. *Knee Surgery, Sports Traumatology, Arthroscopy* **2010**, *18* (4), 419−433.
(45) Sophia Fox, A. J.; Bedi, A.; Rodeo, S. A. The basic science of articular cartilage: Structure, composition, and function. *Sports Health* **2009**, *1* (6), 461−468.
(46) Gottardi, R.; Hansen, U.; Raiteri, R.; Loparic, M.; Düggelin, M.; Mathys, D.; Friederich, N. F.; Bruckner, P.; Stolz, M. Supramolecular Organization of Collagen Fibrils in Healthy and Osteoarthritic Human Knee and Hip Joint Cartilage. *PLoS One* **2016**, *11* (10), e0163552.
(47) Singh, I. The architecture of cancellous bone. *J. Anat.* **1978**, *127* (Pt 2), 305−310.
(48) Mendler, M.; Eich-Bender, S. G.; Vaughan, L.; Winterhalter, K. H.; Bruckner, P. Cartilage contains mixed fibrils of collagen types II, IX, and XI. *J. Cell Biol.* **1989**, *108* (1), 191−7.
(49) Hsueh, M. F.; Khabut, A.; Kjellström, S.; Önnerfjord, P.; Kraus, V. B. Elucidating the Molecular Composition of Cartilage by Proteomics. *J. Proteome Res.* **2016**, *15* (2), 374−88.
(50) Robinson, D. L.; Kersh, M. E.; Walsh, N. C.; Ackland, D. C.; de Steiger, R. N.; Pandy, M. G. Mechanical properties of normal and osteoarthritic human articular cartilage. *Journal of the Mechanical Behavior of Biomedical Materials* **2016**, *61*, 96−109.
(51) Hoemann, C. Molecular and Biochemical Assays of Cartilage Components. *Methods in molecular medicine* **2004**, *101*, 127−56.
(52) Wu, J. J.; Woods, P. E.; Eyre, D. R. Identification of cross-linking sites in bovine cartilage type IX collagen reveals an antiparallel type II-type IX molecular relationship and type IX to type IX bonding. *J. Biol. Chem.* **1992**, *267* (32), 23007−14.
(53) Qu, D.; Mosher, C. Z.; Boushell, M. K.; Lu, H. H. Engineering complex orthopaedic tissues via strategic biomimicry. *Ann. Biomed. Eng.* **2015**, *43* (3), 697−717.
(54) Ralphs, J. R.; Benjamin, M. The joint capsule: structure, composition, ageing and disease. *J. Anat.* **1994**, *184* (Pt 3), 503−509.
(55) Augat, P.; Schorlemmer, S. The role of cortical bone and its microstructure in bone strength. *Age Ageing* **2006**, *35* (Suppl 2), ii27−ii31.
(56) Lai, Y.-S.; Chen, W.-C.; Huang, C.-H.; Cheng, C.-K.; Chan, K.-K.; Chang, T.-K. The Effect of Graft Strength on Knee Laxity and Graft In-Situ Forces after Posterior Cruciate Ligament Reconstruction. *PLoS One* **2015**, *10* (5), e0127293.
(57) Gibson, L. J. The mechanical behaviour of cancellous bone. *J. Biomech.* **1985**, *18* (5), 317−28.
(58) Paxton, J.; Baar, K.; Grover, L. Current progress in enthesis repair: strategies for interfacial tissue engineering. *Orthopedic Muscul. Sys.* **2013**, *1*, DOI: 10.4172/2161-0533.S1-003.
(59) Benjamin, M.; Ralphs, J. R. Fibrocartilage in tendons and ligaments–an adaptation to compressive load. *J. Anat.* **1998**, *193* (Pt 4), 481−494.
(60) Olvera, D.; Sathy, B. N.; Kelly, D. J. Spatial Presentation of Tissue-Specific Extracellular Matrix Components along Electrospun Scaffolds for Tissue Engineering the Bone−Ligament Interface. *ACS Biomater. Sci. Eng.* **2020**, *6* (9), 5145−5161.
(61) Kuntz, L. A.; Rossetti, L.; Kunold, E.; Schmitt, A.; von Eisenhart-Rothe, R.; Bausch, A. R.; Burgkart, R. H. Biomarkers for tissue engineering of the tendon-bone interface. *PLoS One* **2018**, *13* (1), e0189668.
(62) Petermann, H.; Sander, M. Histological evidence for muscle insertion in extant amniote femora: implications for muscle reconstruction in fossils. *J. Anat.* **2013**, *222* (4), 419−436.
(63) Aaron, J. Periosteal Sharpey's Fibres: a Novel Bone Matrix Regulatory System? *Front. Endocrinol.* **2012**, *3*, 98.
(64) Lu, H. H.; Thomopoulos, S. Functional attachment of soft tissues to bone: development, healing, and tissue engineering. *Annu. Rev. Biomed. Eng.* **2013**, *15*, 201−26.
(65) Apostolakos, J.; Durant, T. J.; Dwyer, C. R.; Russell, R. P.; Weinreb, J. H.; Alaee, F.; Beitzel, K.; McCarthy, M. B.; Cote, M. P.; Mazzocca, A. D. The enthesis: a review of the tendon-to-bone insertion. *Muscles, ligaments and tendons journal* **2019**, *4* (3), 333.
(66) Ker, D. F. E.; Wang, D.; Behn, A. W.; Wang, E. T. H.; Zhang, X.; Zhou, B. Y.; Mercado-Pagán, Á. E.; Kim, S.; Kleimeyer, J.; Gharaibeh, B. Functionally Graded, Bone-and Tendon-Like Polyurethane for Rotator Cuff Repair. *Adv. Funct. Mater.* **2018**, *28* (20), 1707107.
(67) Benjamin, M.; Kumai, T.; Milz, S.; Boszczyk, B.; Boszczyk, A. A.; Ralphs, J. The skeletal attachment of tendons—tendon 'entheses'. *Comp. Biochem. Physiol., Part A: Mol. Integr. Physiol.* **2002**, *133* (4), 931−945.
(68) Milz, S.; Rufai, A.; Buettner, A.; Putz, R.; Ralphs, J.; Benjamin, M. Three-dimensional reconstructions of the Achilles tendon insertion in man. *J. Anat.* **2002**, *200* (2), 145−152.
(69) Gao, J.; Messner, K. Quantitative comparison of soft tissue-bone interface at chondral ligament insertions in the rabbit knee joint. *J. Anat.* **1996**, *188*, 367−372.
(70) Zhao, L.; Thambyah, A.; Broom, N. D. A multi-scale structural study of the porcine anterior cruciate ligament tibial enthesis. *J. Anat.* **2014**, *224* (6), 624−633.
(71) Chan, Y. L.; Ngan, A. H.; King, N. M. Nano-scale structure and mechanical properties of the human dentine-enamel junction. *Journal of the mechanical behavior of biomedical materials* **2011**, *4* (5), 785−95.
(72) Thorp, H.; Kim, K.; Kondo, M.; Maak, T.; Grainger, D. W.; Okano, T. Trends in Articular Cartilage Tissue Engineering: 3D Mesenchymal Stem Cell Sheets as Candidates for Engineered Hyaline-Like Cartilage. *Cells* **2021**, *10* (3), 643.
(73) Lynch, H.; Johannessen, W.; Wu, J.; Jawa, A.; Elliott, D. Effect of fiber orientation and strain rate on the nonlinear uniaxial tensile material Properties of Tendon. *J. Biomech. Eng.* **2003**, *125*, 726−31.
(74) Eckstein, F.; Hudelmaier, M.; Putz, R. The effects of exercise on human articular cartilage. *J. Anat.* **2006**, *208* (4), 491−512.

(75) Desmond, K. W.; Zacchia, N. A.; Waite, J. H.; Valentine, M. T. Dynamics of mussel plaque detachment. *Soft Matter* **2015**, *11* (34), 6832−9.
(76) Lee, B. P.; Messersmith, P. B.; Israelachvili, J. N.; Waite, J. H. Mussel-Inspired Adhesives and Coatings. *Annu. Rev. Mater. Res.* **2011**, *41* (1), 99−132.
(77) Banea, M. D.; da Silva, L. F. M. Adhesively bonded joints in composite materials: an overview. *Proc. Inst. Mech. Eng., Part L* **2009**, *223* (1), 1−18.
(78) Ebnesajjad, S.; Landrock, A. H. Chapter 3 - Material Surface Preparation Techniques. In *Adhesives Technology Handbook*, 3rd ed.; Ebnesajjad, S., Landrock, A. H., Eds.; William Andrew Publishing: Boston, 2015; pp 35−66.
(79) Bogy, D. B. Edge-Bonded Dissimilar Orthogonal Elastic Wedges Under Normal and Shear Loading. *J. Appl. Mech.* **1968**, *35* (3), 460−466.
(80) Liu, Y. X.; Thomopoulos, S.; Birman, V.; Li, J. S.; Genin, G. M. Bi-material attachment through a compliant interfacial system at the tendon-to-bone insertion site. *Mech. Mater.* **2012**, *44*, 83−92.
(81) Deymier, A. C.; An, Y.; Boyle, J. J.; Schwartz, A. G.; Birman, V.; Genin, G. M.; Thomopoulos, S.; Barber, A. H. Micro-mechanical properties of the tendon-to-bone attachment. *Acta Biomater.* **2017**, *56*, 25−35.
(82) Liu, Y.; Birman, V.; Chen, C.; Thomopoulos, S.; Genin, G. M. Mechanisms of bimaterial attachment at the interface of tendon to bone. *J. Eng. Mater. Technol.* **2011**, *133* (1), 011006.
(83) Friese, N.; Gierschner, M. B.; Schadzek, P.; Roger, Y.; Hoffmann, A. Regeneration of Damaged Tendon-Bone Junctions (Entheses)—TAK1 as a Potential Node Factor. *Int. J. Mol. Sci.* **2020**, *21* (15), 5177.
(84) Ho, S. P.; Marshall, S. J.; Ryder, M. I.; Marshall, G. W. The tooth attachment mechanism defined by structure, chemical composition and mechanical properties of collagen fibers in the periodontium. *Biomaterials* **2007**, *28* (35), 5238−5245.
(85) Chung, J. Y.; Chaudhury, M. K. Soft and Hard Adhesion. *J. Adhes.* **2005**, *81* (10−11), 1119−1145.
(86) Zhang, Y.; Yao, H.; Ortiz, C.; Xu, J.; Dao, M. Bio-inspired interfacial strengthening strategy through geometrically interlocking designs. *J. Mech Behav Biomed Mater.* **2012**, *15*, 70−7.
(87) Han, L.; Wang, L.; Song, J.; Boyce, M. C.; Ortiz, C. Direct quantification of the mechanical anisotropy and fracture of an individual exoskeleton layer via uniaxial compression of micropillars. *Nano Lett.* **2011**, *11* (9), 3868−74.
(88) Wang, R. Z.; Suo, Z.; Evans, A. G.; Yao, N.; Aksay, I. A. Deformation mechanisms in nacre. *J. Mater. Res.* **2001**, *16* (9), 2485−2493.
(89) Launey, M. E.; Munch, E.; Alsem, D. H.; Barth, H. B.; Saiz, E.; Tomsia, A. P.; Ritchie, R. O. Designing highly toughened hybrid composites through nature-inspired hierarchical complexity. *Acta Mater.* **2009**, *57* (10), 2919−2932.
(90) Eugene Stanley, H. Fractal landscapes in physics and biology. *Phys. A* **1992**, *186* (1), 1−32.
(91) Jaslow, C. R.; Biewener, A. A. Strain patterns in the horncores, cranial bones and sutures of goats (Capra hircus) during impact loading. *J. Zool.* **1995**, *235* (2), 193−210.
(92) De Blasio, F. V. The role of suture complexity in diminishing strain and stress in ammonoid phragmocones. *Lethaia* **2008**, *41* (1), 15−24.
(93) Li, Y.; Ortiz, C.; Boyce, M. C. Bioinspired, mechanical, deterministic fractal model for hierarchical suture joints. *Phys. Rev. E* **2012**, *85* (3Pt 1), 031901.
(94) Li, Y.; Ortiz, C.; Boyce, M. C. Stiffness and strength of suture joints in nature. *Phys. Rev. E* **2011**, *84* (6 Pt 1), 062904.
(95) Lin, E.; Li, Y.; Ortiz, C.; Boyce, M. C. 3D printed, bio-inspired prototypes and analytical models for structured suture interfaces with geometrically-tuned deformation and failure behavior. *J. Mech. Phys. Solids* **2014**, *73*, 166−182.
(96) Li, Y.; Ortiz, C.; Boyce, M. C. A generalized mechanical model for suture interfaces of arbitrary geometry. *J. Mech. Phys. Solids* **2013**, *61* (4), 1144−1167.
(97) Hosseini, M. S.; Cordisco, F. A.; Zavattieri, P. D. Analysis of bioinspired non-interlocking geometrically patterned interfaces under predominant mode I loading. *Journal of the mechanical behavior of biomedical materials* **2019**, *96*, 244−260.
(98) Ahankari, S. S.; Kar, K. K. Functionally Graded Composites: Processing and Applications. In *Composite Materials*; Springer: Berlin, Heidelberg, 2017; pp 119−168.
(99) Mahamood, R. M.; Member, E. T. A.; Shukla, D. M.; Pityana, S. Functionally graded material: An overview. *World Congress on Engineering* **2012**, *3*, 2−6.
(100) Pompe, W.; Worch, H.; Epple, M.; Friess, W.; Gelinsky, M.; Greil, P.; Hempel, U.; Scharnweber, D.; Schulte, K. Functionally graded materials for biomedical applications. *Mater. Sci. Eng., A* **2003**, *362* (1), 40.
(101) Rousseau, M. Nacre, a Natural Biomaterial. In *Biomaterials Applications for Nanomedicine*; Pignatello, R., Ed.; InTech: 2011; pp 281−298.
(102) Fratzl, P.; Gupta, H. S.; Fischer, F. D.; Kolednik, O. Hindered Crack Propagation in Materials with Periodically Varying Young's Modulus—Lessons from Biological Materials. *Adv. Mater.* **2007**, *19* (18), 2657−2661.
(103) Bouville, F.; Stevenson, A. J.; Deville, S.; Maire, E.; Meille, S.; Van De Moortele, B. Strong, tough and stiff bioinspired ceramics from brittle constituents. *Nat. Mater.* **2014**, *13* (5), 508−514.
(104) Mahmoud, D.; Mohamed, A. E. Lattice Structures and Functionally Graded Materials Applications in Additive Manufacturing of Orthopedic Implants: A Review. *J. Manuf. Mater. Process.* **2017**, *1* (2), 13.
(105) Huiskes, R.; Weinans, H.; Van Rietbergen, B. The relationship between stress shielding and bone resorption around total hip stems and the effects of flexible materials. *Clin. Orthop. Relat. Res.* **1992**, 124−134.
(106) Saini, M.; Singh, Y.; Arora, P.; Arora, V.; Jain, K. Implant biomaterials: A comprehensive review. *World J. Clin Cases* **2015**, *3* (1), 52−7.
(107) Ishikawa, K.; Matsuya, S.; Miyamoto, Y.; Kawate, K. 9.05 - Bioceramics. In *Comprehensive Structural Integrity*; Milne, I., Ritchie, R. O., Karihaloo, B., Eds.; Pergamon: Oxford, 2003; pp 169−214.
(108) Jones, J. R.; Lin, S.; Yue, S.; Lee, P. D.; Hanna, J. V.; Smith, M. E.; Newport, R. J. Bioactive glass scaffolds for bone regeneration and their hierarchical characterisation. *Proc. Inst. Mech. Eng., Part H* **2010**, *224* (12), 1373−87.
(109) Mesquita, P.; Branco, R.; Afonso, A.; Vasconcelos, M.; Cavalheiro, J. Mineralised Membranes for Bone Regeneration. *Key Eng. Mater.* **2003**, *254*−*256*, 1091−1094.
(110) Liu, X.; Rahaman, M. N.; Fu, Q. Bone regeneration in strong porous bioactive glass (13−93) scaffolds with an oriented microstructure implanted in rat calvarial defects. *Acta Biomater.* **2013**, *9* (1), 4889−98.
(111) Von Euw, S.; Wang, Y.; Laurent, G.; Drouet, C.; Babonneau, F.; Nassif, N.; Azais, T. Bone mineral: new insights into its chemical composition. *Sci. Rep.* **2019**, *9* (1), 8456.
(112) Sunho, O.; Namsik, O.; Mark, A.; Joo, L. O. Bioceramics for Tissue Engineering Applications − A Review. *Am. J. Biochem. Biotechnol.* **2006**, *2*, 49−56.
(113) Milazzo, M.; Contessi Negrini, N.; Scialla, S.; Marelli, B.; Farè, S.; Danti, S.; Buehler, M. J. Additive Manufacturing Approaches for Hydroxyapatite-Reinforced Composites. *Adv. Funct. Mater.* **2019**, *29* (35), 1903055.
(114) Balani, K.; Verma, V.; Agarwal, A.; Narayan, R. *Biosurfaces: a Materials Science and Engineering Perspective*; John Wiley & Sons: 2015.
(115) Ding, C.; Qiao, Z.; Jiang, W.; Li, H.; Wei, J.; Zhou, G.; Dai, K. Regeneration of a goat femoral head using a tissue-specific, biphasic scaffold fabricated with CAD/CAM technology. *Biomaterials* **2013**, *34* (28), 6706−16.

https://doi.org/10.1021/acsbiomaterials.1c00620
ACS Biomater. Sci. Eng. 2023, 9, 3810−3831

(116) Castro, N. J.; O'Brien, C. M.; Zhang, L. G. Biomimetic biphasic 3-D nanocomposite scaffold for osteochondral regeneration. *AIChE J.* **2014**, *60* (2), 432−442.
(117) Erisken, C.; Kalyon, D. M.; Wang, H. Functionally graded electrospun polycaprolactone and b-tricalcium phosphate nanocomposites for tissue engineering applications. *Biomaterials* **2008**, *29* (30), 4065−4073.
(118) Barbeck, M.; Serra, T.; Booms, P.; Stojanovic, S.; Najman, S.; Engel, E.; Sader, R.; Kirkpatrick, C. J.; Navarro, M.; Ghanaati, S. Analysis of the in vitro degradation and the in vivo tissue response to bi-layered 3D-printed scaffolds combining PLA and biphasic PLA/bioglass components - Guidance of the inflammatory response as basis for osteochondral regeneration. *Bioactive materials* **2017**, *2* (4), 208−223.
(119) Hajiali, F.; Tajbakhsh, S.; Shojaei, A. Fabrication and Properties of Polycaprolactone Composites Containing Calcium Phosphate-Based Ceramics and Bioactive Glasses in Bone Tissue Engineering: A Review. *Polym. Rev.* **2018**, *58* (1), 164−207.
(120) Shalumon, K. T.; Sheu, C.; Fong, Y. T.; Liao, H.-T.; Chen, J.-P. Microsphere-Based Hierarchically Juxtapositioned Biphasic Scaffolds Prepared from Poly(Lactic-co-Glycolic Acid) and Nanohydroxyapatite for Osteochondral Tissue Engineering. *Polymers* **2016**, *8* (12), 429.
(121) Schaefer, D.; Martin, I.; Shastri, P.; Padera, R. F.; Langer, R.; Freed, L. E.; Vunjak-Novakovic, G. In vitro generation of osteochondral composites. *Biomaterials* **2000**, *21* (24), 2599−2606.
(122) Astete, C.; Sabliov, C. Synthesis and characterization of PLGA nanoparticles. *J. Biomater. Sci., Polym. Ed.* **2006**, *17* (3), 247−289.
(123) Tahriri, M.; Moztarzadeh, F. Preparation, characterization, and in vitro biological evaluation of PLGA/nano-fluorohydroxyapatite (FHA) microsphere-sintered scaffolds for biomedical applications. *Appl. Biochem. Biotechnol.* **2014**, *172* (5), 2465−79.
(124) Dwivedi, R.; Kumar, S.; Pandey, R.; Mahajan, A.; Nandana, D.; Katti, D. S.; Mehrotra, D. Polycaprolactone as biomaterial for bone scaffolds: Review of literature. *Journal of Oral Biology and Craniofacial Research* **2020**, *10* (1), 381−388.
(125) Wong, B. L.; Sah, R. L. Mechanical asymmetry during articulation of tibial and femoral cartilages: local and overall compressive and shear deformation and properties. *J. Biomech.* **2010**, *43* (9), 1689−1695.
(126) Abdullah, S. Usage of synthetic tendons in tendon reconstruction. *BMC Proc.* **2015**, *9* (Suppl 3), A68−A68.
(127) Senatov, F. S.; Kopylov, A. N.; Anisimova, N. Y.; Kiselevsky, M. V.; Maksimkin, A. V. UHMWPE-based nanocomposite as a material for damaged cartilage replacement. *Mater. Sci. Eng., C* **2015**, *48*, 566−571.
(128) Wagner, E. R.; Parry, J.; Dadsetan, M.; Bravo, D.; Riester, S. M.; van Wijnen, A. J.; Yaszemski, M. J.; Kakar, S. Chondrocyte Attachment, Proliferation, and Differentiation on Three-Dimensional Polycaprolactone Fumarate Scaffolds. *Tissue Eng., Part A* **2017**, *23* (13−14), 622−629.
(129) Medvedeva, E. V.; Grebenik, E. A.; Gornostaeva, S. N.; Telpuhov, V. I.; Lychagin, A. V.; Timashev, P. S.; Chagin, A. S. Repair of Damaged Articular Cartilage: Current Approaches and Future Directions. *Int. J. Mol. Sci.* **2018**, *19* (8), 2366.
(130) Frenkel, S. R.; Bradica, G.; Brekke, J. H.; Goldman, S. M.; Ieska, K.; Issack, P.; Bong, M. R.; Tian, H.; Gokhale, J.; Coutts, R. D.; Kronengold, R. T. Regeneration of articular cartilage–evaluation of osteochondral defect repair in the rabbit using multiphasic implants. *Osteoarthritis Cartilage* **2005**, *13* (9), 798−807.
(131) Diduch, D. R.; Jordan, L. C.; Mierisch, C. M.; Balian, G. Marrow stromal cells embedded in alginate for repair of osteochondral defects. *Arthroscopy* **2000**, *16* (6), 571−7.
(132) Mohan, N.; Gupta, V.; Sridharan, B.; Sutherland, A.; Detamore, M. S. The potential of encapsulating "raw materials" in 3D osteochondral gradient scaffolds. *Biotechnol. Bioeng.* **2014**, *111* (4), 829−841.
(133) Gao, J.; Dennis, J. E.; Solchaga, L. A.; Goldberg, V. M.; Caplan, A. I. Repair of osteochondral defect with tissue-engineered two-phase composite material of injectable calcium phosphate and hyaluronan sponge. *Tissue Eng.* **2002**, *8* (5), 827−37.
(134) Li, J.; Mareddy, S.; Tan, D. M.; Crawford, R.; Long, X.; Miao, X.; Xiao, Y. A minimal common osteochondrocytic differentiation medium for the osteogenic and chondrogenic differentiation of bone marrow stromal cells in the construction of osteochondral graft. *Tissue Eng., Part A* **2009**, *15* (9), 2481−90.
(135) Cao, Z.; Hou, S.; Sun, D.; Wang, X.; Tang, J. Osteochondral regeneration by a bilayered construct in a cell-free or cell-based approach. *Biotechnol. Lett.* **2012**, *34* (6), 1151−7.
(136) Guo, X.; Park, H.; Liu, G.; Liu, W.; Cao, Y.; Tabata, Y.; Kasper, F. K.; Mikos, A. G. In vitro generation of an osteochondral construct using injectable hydrogel composites encapsulating rabbit marrow mesenchymal stem cells. *Biomaterials* **2009**, *30* (14), 2741−52.
(137) Cunniffe, G. M.; Díaz-Payno, P. J.; Sheehy, E. J.; Critchley, S. E.; Almeida, H. V.; Pitacco, P.; Carroll, S. F.; Mahon, O. R.; Dunne, A.; Levingstone, T. J.; Moran, C. J.; Brady, R. T.; O'Brien, F. J.; Brama, P. A. J.; Kelly, D. J. Tissue-specific extracellular matrix scaffolds for the regeneration of spatially complex musculoskeletal tissues. *Biomaterials* **2019**, *188*, 63−73.
(138) Dua, R.; Centeno, J.; Ramaswamy, S. Augmentation of engineered cartilage to bone integration using hydroxyapatite. *J. Biomed. Mater. Res., Part B* **2014**, *102* (5), 922−932.
(139) Burla, F.; Tauber, J.; Dussi, S.; van Der Gucht, J.; Koenderink, G. H. Stress management in composite biopolymer networks. *Nat. Phys.* **2019**, *15* (6), 549−553.
(140) Baldino, L.; Maffulli, N.; Reverchon, E. 14 - Bone−tendon interface. In *Regenerative Engineering of Musculoskeletal Tissues and Interfaces*; Nukavarapu, S. P., Freeman, J. W., Laurencin, C. T., Eds.; Woodhead Publishing: 2015; pp 345−361.
(141) Amini, A. R.; Laurencin, C. T.; Nukavarapu, S. P. Bone tissue engineering: recent advances and challenges. *Critical reviews in biomedical engineering* **2012**, *40* (5), 363−408.
(142) Beldjilali-Labro, M.; Garcia Garcia, A.; Farhat, F.; Bedoui, F.; Grosset, J. F.; Dufresne, M.; Legallais, C., Biomaterials in Tendon and Skeletal Muscle Tissue Engineering: Current Trends and Challenges. *Materials* **2018**, *11* (7), 1116.
(143) Laurent, C. d.; Liu, X.; De Isla, N.; Wang, X.; Rahouadj, R. Defining a scaffold for ligament tissue engineering: What has been done, and what still needs to be done. *Journal of Cellular Immunotherapy* **2018**, *4* (1), 4−9.
(144) Qazi, T. H.; Mooney, D. J.; Pumberger, M.; Geißler, S.; Duda, G. N. Biomaterials based strategies for skeletal muscle tissue engineering: Existing technologies and future trends. *Biomaterials* **2015**, *53*, 502−521.
(145) Casanellas, I.; García-Lizarribar, A.; Lagunas, A.; Samitier, J. Producing 3D Biomimetic Nanomaterials for Musculoskeletal System Regeneration. *Front. Bioeng. Biotechnol.* **2018**, *6*, 128.
(146) Thomopoulos, S.; Birman, V.; Genin, G. M. *Structural interfaces and attachments in biology*; Springer, Science & Business Media: New York, NY, 2013.
(147) Loh, G. H.; Pei, E.; Harrison, D.; Monzón, M. D. An overview of functionally graded additive manufacturing. *Additive Manufacturing* **2018**, *23*, 34−44.
(148) Sun, M.; Chi, G.; Li, P.; Lv, S.; Xu, J.; Xu, Z.; Xia, Y.; Tan, Y.; Xu, J.; Li, L.; Li, Y. Effects of Matrix Stiffness on the Morphology, Adhesion, Proliferation and Osteogenic Differentiation of Mesenchymal Stem Cells. *Int. J. Med. Sci.* **2018**, *15* (3), 257−268.
(149) Mullen, C. A.; Vaughan, T. J.; Billiar, K. L.; McNamara, L. M. The effect of substrate stiffness, thickness, and cross-linking density on osteogenic cell behavior. *Biophys. J.* **2015**, *108* (7), 1604−1612.
(150) Ehrbar, M.; Sala, A.; Lienemann, P.; Ranga, A.; Mosiewicz, K.; Bittermann, A.; Rizzi, S. C.; Weber, F. E.; Lutolf, M. P. Elucidating the role of matrix stiffness in 3D cell migration and remodeling. *Biophys. J.* **2011**, *100* (2), 284−93.
(151) Charrier, E. E.; Pogoda, K.; Wells, R. G.; Janmey, P. A. Control of cell morphology and differentiation by substrates with

https://doi.org/10.1021/acsbiomaterials.1c00620
ACS Biomater. Sci. Eng. 2023, 9, 3810−3831

independently tunable elasticity and viscous dissipation. *Nat. Commun.* **2018**, *9* (1), 449.
(152) Olivares-Navarrete, R.; Lee, E. M.; Smith, K.; Hyzy, S. L.; Doroudi, M.; Williams, J. K.; Gall, K.; Boyan, B. D.; Schwartz, Z. Substrate Stiffness Controls Osteoblastic and Chondrocytic Differentiation of Mesenchymal Stem Cells without Exogenous Stimuli. *PLoS One* **2017**, *12* (1), e0170312.
(153) Obbink-Huizer, C.; Oomens, C. W.; Loerakker, S.; Foolen, J.; Bouten, C. V.; Baaijens, F. P. Computational model predicts cell orientation in response to a range of mechanical stimuli. *Biomech. Model. Mechanobiol.* **2014**, *13* (1), 227−36.
(154) Chen, K.; Vigliotti, A.; Bacca, M.; McMeeking, R. M.; Deshpande, V. S.; Holmes, J. W. Role of boundary conditions in determining cell alignment in response to stretch. *Proc. Natl. Acad. Sci. U. S. A.* **2018**, *115* (5), 986.
(155) Bischofs, I.; Schwarz, U. Cell organization in soft media due to active mechanosensing. *Proc. Natl. Acad. Sci. U. S. A.* **2003**, *100*, 9274−9.
(156) Bell, E.; Ivarsson, B.; Merrill, C. Production of a tissue-like structure by contraction of collagen lattices by human fibroblasts of different proliferative potential in vitro. *Proc. Natl. Acad. Sci. U. S. A.* **1979**, *76* (3), 1274−1278.
(157) Harris, A. K.; Stopak, D.; Wild, P. Fibroblast traction as a mechanism for collagen morphogenesis. *Nature* **1981**, *290* (5803), 249−51.
(158) Petroll, W. M.; Cavanagh, H. D.; Jester, J. V. Dynamic three-dimensional visualization of collagen matrix remodeling and cytoskeletal organization in living corneal fibroblasts. *Scanning* **2004**, *26* (1), 1−10.
(159) Ploetz, C.; Zycband, E.; Birk, D. Collagen fibril assembly and deposition in the developing dermis: Segmental deposition in extracellular compartments. *J. Struct. Biol.* **1991**, *106*, 73−81.
(160) Yannas, I. V. Similarities and differences between induced organ regeneration in adults and early foetal regeneration. *J. R. Soc., Interface* **2005**, *2* (5), 403−417.
(161) Luo, L.; Chu, J.; Eswaramoorthy, R.; Mulhall, K.; Kelly, D. Engineering Tissues That Mimic the Zonal Nature of Articular Cartilage Using Decellularized Cartilage Explants Seeded with Adult Stem Cells. *ACS Biomater. Sci. Eng.* **2017**, *3* (9), 1933−1943.
(162) Petersen, A.; Princ, A.; Korus, G.; Ellinghaus, A.; Leemhuis, H.; Herrera, A.; Klaumünzer, A.; Schreivogel, S.; Woloszyk, A.; Schmidt-Bleek, K.; Geissler, S.; Heschel, I.; Duda, G. N. A biomaterial with a channel-like pore architecture induces endochondral healing of bone defects. *Nat. Commun.* **2018**, *9* (1), 4430.
(163) Olvera, D.; Sathy, B. N.; Carroll, S. F.; Kelly, D. J. Modulating microfibrillar alignment and growth factor stimulation to regulate mesenchymal stem cell differentiation. *Acta Biomater.* **2017**, *64*, 148−160.
(164) Pauly, H.; Nelson Sathy, B.; Olvera, D.; McCarthy, H.; Kelly, D.; Popat, K.; Dunne, N.; Donahue, T. Hierarchically Structured Electrospun Scaffolds with Chemically Conjugated Growth Factor for Ligament Tissue Engineering. *Tissue Engineering Part A* **Aug 2017**, *23* (15−16), 823−836.
(165) Rowland, C. R.; Colucci, L. A.; Guilak, F. Fabrication of anatomically-shaped cartilage constructs using decellularized cartilage-derived matrix scaffolds. *Biomaterials* **2016**, *91*, 57−72.
(166) Zhang, T.; Zhang, H.; Zhang, L.; Jia, S.; Liu, J.; Xiong, Z.; Sun, W. Biomimetic design and fabrication of multilayered osteochondral scaffolds by low-temperature deposition manufacturing and thermal-induced phase-separation techniques. *Biofabrication* **2017**, *9*, 025021.
(167) Domingues, R. M.; Chiera, S.; Gershovich, P.; Motta, A.; Reis, R. L.; Gomes, M. E. Enhancing the Biomechanical Performance of Anisotropic Nanofibrous Scaffolds in Tendon Tissue Engineering: Reinforcement with Cellulose Nanocrystals. *Adv. Healthcare Mater.* **2016**, *5* (11), 1364−75.
(168) Pauly, H.; Nelson Sathy, B.; Olvera, D.; McCarthy, H.; Kelly, D.; Popat, K.; Dunne, N.; Donahue, T. Hierarchically Structured Electrospun Scaffolds with Chemically Conjugated Growth Factor for Ligament Tissue Engineering. *Tissue Engineering Part A* **Aug 2017**, *23* (15−16), 823−836.
(169) Jia, S.; Zhang, T.; Xiong, Z.; Pan, W.; Liu, J.; Sun, W. In Vivo Evaluation of a Novel Oriented Scaffold-BMSC Construct for Enhancing Full-Thickness Articular Cartilage Repair in a Rabbit Model. *PLoS One* **2015**, *10* (12), e0145667.
(170) Ibrahim, N. S.; Krishnamurithy, G.; Rao Balaji Raghavendran, H.; Puvaneswary, S.; Wuey Min, N.; Kamarul, T. Novel HA-PVA/NOCC bilayered scaffold for osteochondral tissue-engineering applications - Fabrication, characterization, in vitro and in vivo biocompatibility study. *Mater. Lett.* **2013**, *113*, 25−29.
(171) Pauly, H.; Nelson Sathy, B.; Olvera, D.; McCarthy, H.; Kelly, D.; Popat, K.; Dunne, N.; Donahue, T. Hierarchically Structured Electrospun Scaffolds with Chemically Conjugated Growth Factor for Ligament Tissue Engineering. *Tissue Eng. Part A* **2017**, *23* (15−16), 823−836.
(172) Galperin, A.; Oldinski, R. A.; Florczyk, S. J.; Bryers, J. D.; Zhang, M.; Ratner, B. D. Integrated Bi-Layered Scaffold for Osteochondral Tissue Engineering. *Adv. Healthcare Mater.* **2013**, *2* (6), 872−883.
(173) Ding, X.; Zhu, M.; Xu, B.; Zhang, J.; Zhao, Y.; Ji, S.; Wang, L.; Li, X.; Kong, D.; Ma, X.; Yang, Q. Integrated trilayered silk fibroin scaffold for osteochondral differentiation of adipose-derived stem cells. *ACS Appl. Mater. Interfaces* **2014**, *6* (19), 16696−705.
(174) Zhou, T.; Wu, J.; Liu, J.; Luo, Y.; Wan, Y. Fabrication and characterization of layered chitosan/silk fibroin/nano-hydroxyapatite scaffolds with designed composition and mechanical properties. *Biomedical materials (Bristol, England)* **2015**, *10* (4), 045013.
(175) Granito, R. N.; Muniz Renno, A. C.; Yamamura, H.; de Almeida, M. C.; Menin Ruiz, P. L.; Ribeiro, D. A. Hydroxyapatite from Fish for Bone Tissue Engineering: A Promising Approach. *Int. J. Mol. Cell. Med.* **2018**, *7* (2), 80−90.
(176) Zhou, H.; Lee, J. Nanoscale hydroxyapatite particles for bone tissue engineering. *Acta Biomater.* **2011**, *7* (7), 2769−81.
(177) Khanarian, N. T.; Haney, N. M.; Burga, R. A.; Lu, H. H. A functional agarose-hydroxyapatite scaffold for osteochondral interface regeneration. *Biomaterials* **2012**, *33* (21), 5247−5258.
(178) Chen, J.; Chen, H.; Li, P.; Diao, H.; Zhu, S.; Dong, L.; Wang, R.; Guo, T.; Zhao, J.; Zhang, J. Simultaneous regeneration of articular cartilage and subchondral bone in vivo using MSCs induced by a spatially controlled gene delivery system in bilayered integrated scaffolds. *Biomaterials* **2011**, *32* (21), 4793−805.
(179) Gao, F.; Xu, Z.; Liang, Q.; Li, H.; Peng, L.; Wu, M.; Zhao, X.; Cui, X.; Ruan, C.; Liu, W. Osteochondral Regeneration with 3D-Printed Biodegradable High-Strength Supramolecular Polymer Reinforced-Gelatin Hydrogel Scaffolds. *Advanced Science* **2019**, *6*, 1900867.
(180) Canadas, R. l. F.; Ren, T.; Marques, A. P.; Oliveira, J. M.; Reis, R. L.; Demirci, U. Biochemical Gradients to Generate 3D Heterotypic-Like Tissues with Isotropic and Anisotropic Architectures. *Adv. Funct. Mater.* **2018**, *28* (48), 1804148.
(181) Gelse, K.; Pöschl, E.; Aigner, T. Collagens—structure, function, and biosynthesis. *Adv. Drug Delivery Rev.* **2003**, *55* (12), 1531−1546.
(182) Liu, C.; Han, Z.; Czernuszka, J. T. Gradient collagen/nanohydroxyapatite composite scaffold: Development and characterization. *Acta Biomater.* **2009**, *5* (2), 661−669.
(183) Daly, A. C.; Critchley, S. E.; Rencsok, E. M.; Kelly, D. J. A comparison of different bioinks for 3D bioprinting of fibrocartilage and hyaline cartilage. *Biofabrication* **2016**, *8* (4), 045002.
(184) Chocholata, P.; Kulda, V.; Babuska, V. Fabrication of Scaffolds for Bone-Tissue Regeneration. *Materials* **2019**, *12* (4), 568.
(185) Shah, R. B.; Schwendeman, S. P. A biomimetic approach to active self-microencapsulation of proteins in PLGA. *J. Controlled Release* **2014**, *196*, 60−70.
(186) Ma, X.; Qu, X.; Zhu, W.; Li, Y.-S.; Yuan, S.; Zhang, H.; Liu, J.; Wang, P.; Lai, C. S. E.; Zanella, F.; Feng, G.-S.; Sheikh, F.; Chien, S.; Chen, S. Deterministically patterned biomimetic human iPSC-derived

https://doi.org/10.1021/acsbiomaterials.1c00620
ACS Biomater. Sci. Eng. 2023, 9, 3810−3831

hepatic model via rapid 3D bioprinting. *Proc. Natl. Acad. Sci. U. S. A.* **2016**, *113* (8), 2206−2211.
(187) Dimaraki, A.; Díaz-Payno, P. J.; Minneboo, M.; Nouri-Goushki, M.; Hosseini, M.; Kops, N.; Narcisi, R.; Mirzaali, M. J.; Osch, G. J. V. M. v.; Fratila-Apachitei, L. E.; Zadpoor, A. A. Bioprinting of a Zonal-Specific Cell Density Scaffold: A Biomimetic Approach for Cartilage Tissue Engineering. *Appl. Sci.* **2021**, *11* (17), 7821.
(188) Nowicki, M. A.; Castro, N. J.; Plesniak, M. W.; Zhang, L. G. 3D printing of novel osteochondral scaffolds with graded microstructure. *Nanotechnology* **2016**, *27* (41), 414001.
(189) Critchley, S.; Sheehy, E. J.; Cunniffe, G.; Diaz-Payno, P.; Carroll, S. F.; Jeon, O.; Alsberg, E.; Brama, P. A. J.; Kelly, D. J. 3D printing of fibre-reinforced cartilaginous templates for the regeneration of osteochondral defects. *Acta Biomater.* **2020**, *113*, 130−143.
(190) Paxton, J. Z.; Grover, L. M.; Baar, K. Engineering an in vitro model of a functional ligament from bone to bone. *Tissue Eng., Part A* **2010**, *16* (11), 3515−25.
(191) Font Tellado, S.; Bonani, W.; Balmayor, E. R.; Foehr, P.; Motta, A.; Migliaresi, C.; van Griensven, M. Fabrication and Characterization of Biphasic Silk Fibroin Scaffolds for Tendon/Ligament-to-Bone Tissue Engineering. *Tissue Eng., Part A* **2017**, *23* (15−16), 859−872.
(192) Liu, H.; Yang, L.; Zhang, E.; Cai, D.; Zhu, S.; Bunpetch, V.; Cai, Y.; Hu, Y.; Chen, X.; Ouyang, H.; Zhang, R.; Ran, J.; Dai, X.; Heng, B. C. Biomimetic tendon extracellular matrix composite gradient scaffold enhances ligament-to-bone junction reconstruction. *Acta Biomater.* **2017**, *56*, 129−140.
(193) Sant, S.; Coutinho, D. F.; Gaharwar, A. K.; Neves, N. M.; Reis, R. L.; Gomes, M. E.; Khademhosseini, A. Self-Assembled Hydrogel Fiber Bundles from Oppositely Charged Polyelectrolytes Mimic Micro-/Nanoscale Hierarchy of Collagen. *Adv. Funct. Mater.* **2017**, *27* (36), 1606273.
(194) Spalazzi, J. P.; Dagher, E.; Doty, S. B.; Guo, X. E.; Rodeo, S. A.; Lu, H. H. In vivo evaluation of a multiphased scaffold designed for orthopaedic interface tissue engineering and soft tissue-to-bone integration. *J. Biomed. Mater. Res., Part A* **2008**, *86A* (1), 1−12.
(195) Mosher, C. Z.; Spalazzi, J. P.; Lu, H. H. Stratified scaffold design for engineering composite tissues. *Methods (Amsterdam, Neth.)* **2015**, *84*, 99−102.
(196) Liu, W.; Lipner, J.; Xie, J.; Manning, C. N.; Thomopoulos, S.; Xia, Y. Nanofiber scaffolds with gradients in mineral content for spatial control of osteogenesis. *ACS Appl. Mater. Interfaces* **2014**, *6* (4), 2842−9.
(197) Nowlin, J.; Bismi, M. A.; Delpech, B.; Dumas, P.; Zhou, Y.; Tan, G. Z. Engineering the hard−soft tissue interface with random-to-aligned nanofiber scaffolds. *Nanobiomedicine* **2018**, DOI: 10.1177/1849543518803538.
(198) Ramalingam, M.; Young, M. F.; Thomas, V.; Sun, L.; Chow, L. C.; Tison, C. K.; Chatterjee, K.; Miles, W. C.; Simon, C. G., Jr. Nanofiber scaffold gradients for interfacial tissue engineering. *J. Biomater. Appl.* **2013**, *27* (6), 695−705.
(199) Kolluru, P. V.; Lipner, J.; Liu, W.; Xia, Y.; Thomopoulos, S.; Genin, G. M.; Chasiotis, I. Strong and tough mineralized PLGA nanofibers for tendon-to-bone scaffolds. *Acta Biomater.* **2013**, *9* (12), 9442−9450.
(200) Lipner, J.; Boyle, J.; Thomopoulos, S.; Liu, Y.; Genin, G. M.; Liu, W.; Xia, Y. The mechanics of PLGA nanofiber scaffolds with biomimetic gradients in mineral for tendon-to-bone repair. *Journal of the Mechanical Behavior of Biomedical Materials* **2014**, *40* (1), 59−68.
(201) Kim, B. S.; Kim, E. J.; Choi, J. S.; Jeong, J. H.; Jo, C. H.; Cho, Y. W. Human collagen-based multilayer scaffolds for tendon-to-bone interface tissue engineering. *J. Biomed. Mater. Res., Part A* **2014**, *102* (11), 4044−54.
(202) Paxton, J. Z.; Donnelly, K.; Keatch, R. P.; Baar, K. Engineering the bone-ligament interface using polyethylene glycol diacrylate incorporated with hydroxyapatite. *Tissue Eng., Part A* **2009**, *15* (6), 1201−9.
(203) Li, H.; Fan, J.; Sun, L.; Liu, X.; Cheng, P.; Fan, H. Functional regeneration of ligament-bone interface using a triphasic silk-based graft. *Biomaterials* **2016**, *106*, 180−192.
(204) Samavedi, S.; Olsen Horton, C.; Guelcher, S. A.; Goldstein, A. S.; Whittington, A. R. Fabrication of a model continuously graded co-electrospun mesh for regeneration of the ligament-bone interface. *Acta Biomater.* **2011**, *7* (12), 4131−4138.
(205) Samavedi, S.; Guelcher, S. A.; Goldstein, A. S.; Whittington, A. R. Response of bone marrow stromal cells to graded co-electrospun scaffolds and its implications for engineering the ligament-bone interface. *Biomaterials* **2012**, *33* (31), 7727−7735.
(206) Spalazzi, J. P.; Doty, S. B.; Moffat, K. L.; Levine, W. N.; Lu, H. H. Development of controlled matrix heterogeneity on a triphasic scaffold for orthopedic interface tissue engineering. *Tissue Eng.* **2006**, *12* (12), 3497−508.
(207) Lu, H. H.; Spalazzi, J. P. Biomimetic stratified scaffold design for ligament-to-bone interface tissue engineering. *Comb. Chem. High Throughput Screening* **2009**, *12* (6), 589−97.
(208) Harris, E.; Liu, Y.; Cunniffe, G.; Morrissey, D.; Carroll, S.; Mulhall, K.; Kelly, D. J. Biofabrication of soft tissue templates for engineering the bone-ligament interface. *Biotechnol. Bioeng.* **2017**, *114* (10), 2400−2411.
(209) Moffat, K. L.; Kwei, A. S. P.; Spalazzi, J. P.; Doty, S. B.; Levine, W. N.; Lu, H. H. Novel nanofiber-based scaffold for rotator cuff repair and augmentation. *Tissue Eng., Part A* **2009**, *15* (1), 115−126.
(210) Xie, J.; Li, X.; Lipner, J.; Manning, C. N.; Schwartz, A. G.; Thomopoulos, S.; Xia, Y. "Aligned-to-random" nanofiber scaffolds for mimicking the structure of the tendon-to-bone insertion site. *Nanoscale* **2010**, *2* (6), 923−6.
(211) Xie, J.; Ma, B.; Michael, P. L.; Shuler, F. D. Fabrication of nanofiber scaffolds with gradations in fiber organization and their potential applications. *Macromol. Biosci.* **2012**, *12* (10), 1336−1341.
(212) Samavedi, S.; Vaidya, P.; Gaddam, P.; Whittington, A. R.; Goldstein, A. S. Electrospun meshes possessing region-wise differences in fiber orientation, diameter, chemistry and mechanical properties for engineering bone-ligament-bone tissues. *Biotechnol. Bioeng.* **2014**, *111* (12), 2549−2559.
(213) Criscenti, G.; Longoni, A.; Di Luca, A.; De Maria, C.; van Blitterswijk, C. A.; Vozzi, G.; Moroni, L. Triphasic scaffolds for the regeneration of the bone-ligament interface. *Biofabrication* **2016**, *8* (1), 015009.
(214) Sun Han Chang, R. A.; Shanley, J. F.; Kersh, M. E.; Harley, B. A. C. Tough and tunable scaffold-hydrogel composite biomaterial for soft-to-hard musculoskeletal tissue interfaces. *Sci. Adv.* **2020**, *6* (34), eabb6763.
(215) Bhardwaj, N.; Kundu, S. C. Electrospinning: A fascinating fiber fabrication technique. *Biotechnol. Adv.* **2010**, *28* (3), 325−347.
(216) Yang, G. Z.; Li, H. P.; Yang, J. H.; Wan, J.; Yu, D. G. Influence of Working Temperature on The Formation of Electrospun Polymer Nanofibers. *Nanoscale Res. Lett.* **2017**, *12*, 15.
(217) Abel, S. B.; Liverani, L.; Boccaccini, A. R.; Abraham, G. A. Effect of benign solvents composition on poly(ε-caprolactone) electrospun fiber properties. *Mater. Lett.* **2019**, *245*, 86−89.
(218) Puppi, D.; Chiellini, F. Wet-spinning of biomedical polymers: from single-fibre production to additive manufacturing of three-dimensional scaffolds. *Polym. Int.* **2017**, *66* (12), 1690−1696.
(219) Rider, P.; Kačarević, Z. e. P.; Alkildani, S.; Retnasingh, S.; Barbeck, M. Bioprinting of tissue engineering scaffolds. *J. Tissue Eng.* **2018**, DOI: 10.1177/2041731418802090.